

Photodegradation Pathways of Protein Disulfides: Human Growth Hormone

Daniel Steinmann^{1,2} · Olivier Mozziconacci^{1,3} · Rupesh Bommana¹ · John F. Stobaugh¹ · Y. John Wang⁴ · Christian Schöneich¹ 

Received: 23 June 2017 / Accepted: 5 September 2017 / Published online: 18 September 2017
© Springer Science+Business Media, LLC 2017

ABSTRACT

Purpose Comprehensive product characterization was performed for the photodegradation of protein disulfides, representatively of human growth hormone (somatotropin; hGH), in order to provide a product database, which will be useful for the general analysis of protein stability.

Methods hGH was photo-irradiated at $\lambda = 254$ and $\lambda > 295$ nm and tryptic digests were analyzed by HPLC-MS to investigate light-induced disulfide degradation pathways.

Results A total of 60 products were detected, and structures/tentative structures were assigned to the products by MS² and MS³ analysis. The main products were reduced Cys residues, dithiohemiacetal, thioether and disulfide scrambling products. In addition, we detected Cys degradation products such as Cys thioaldehyde, dehydroalanine (Dha), Ala, Ser semialdehyde, Ser, S-sulfocysteine, and Gly. Frequently, the tryptic fragments contained more than one modification, i.e. a Cys degradation product in close proximity to a dehydrated amino acid. Several novel cross-links were detected between Cys and Tyr, Cys, Ser and Phe, Cys and Trp, and Trp and Tyr. Photo-induced protein fragmentation was detected specifically at or

in close proximity to the disulfide bond between T6 and T16. An in-house packed 75 cm nano-column enabled us to resolve various isomers/diastereomers of the photo-degradation products.

Conclusion A comprehensive analysis of photodegradation products revealed a variety of novel photo-products, including cross-links, originating from disulfide degradation. The mechanisms of product formation are discussed.

KEY WORDS cross-link · disulfide · hGH · human growth hormone · oxidation · peptide cleavage · photo-degradation · somatotropin · thiy radical

ABBREVIATIONS

ACN	Acetonitrile
BMS	Bis(2-mercaptoethyl)sulfone
Dha	Dehydroalanine
hGH	Human growth hormone
IAA	Iodoacetamide
LTQ-FT-ICR	Linear ion trap Fourier transform-ion cyclotron resonance
NEM	N-ethylmaleimide
SerSA	Serine semialdehyde
TIC	Total ion count
XUPLC	Extreme ultrahighperformance liquid chromatography

Electronic supplementary material The online version of this article (<https://doi.org/10.1007/s11095-017-2256-6>) contains supplementary material, which is available to authorized users.

✉ Christian Schöneich
schoneic@ku.edu

¹ Department of Pharmaceutical Chemistry, University of Kansas, 2095 Constant Ave, Lawrence, Kansas 66047, USA

² Present address: Coriolis Pharma, Biopharmaceutical Research and Development Service, Am Klopferspitz 19 D-82152 Martinsried, Germany

³ Present address: Merck Research Laboratories, Rahway, New Jersey 07065, USA

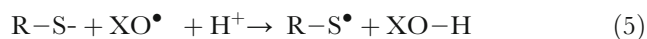
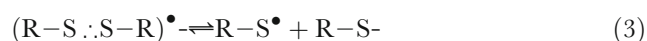
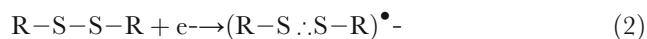
⁴ Late Stage Pharmaceutical Development, Genentech, South San Francisco, California 94080, USA

INTRODUCTION

Protein pharmaceuticals may be exposed to ambient and some UV light during production, formulation and storage, which can lead to protein degradation (1–4), and potentially affect the potency of a formulation. For instance, the photo-irradiation of monoclonal antibodies can lead to aggregation (3–6), oxidation (4,7), fragmentation (8) and reduced

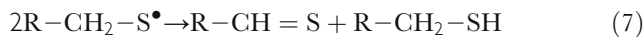
bioactivity (3,5). To assess, predict and prevent such detrimental protein degradation a detailed understanding of product formation and the chemical mechanisms of photodegradation is crucial. For mechanistic studies, we have subjected a small model protein, hGH, to photo-irradiation at $\lambda = 254$ nm and $\lambda > 295$ nm. These wavelengths were selected as an investigative tool (9) to generate a maximal amount and manifold of photo-degradation products within a reasonable experimental time frame. Specifically, wavelengths of $\lambda > 295$ nm overlap with the UV spectrum of Trp, which can extend to $\lambda = 320$ nm (10). Trp has been shown to be sensitive to photo-degradation not only by UV light (11) but also by ambient light (4), and photo-induced electron transfer from Trp can lead to disulfide degradation (12–16). The photo-degradation products identified in this study will provide protein and formulation scientists with a database for the characterization of proteins and/or protein pharmaceuticals exposed to milder stress conditions (e.g., ambient light) or simply long-term storage.

Aromatic amino acids and disulfides are the main chromophores in a protein and are, therefore, predisposed for photodegradation (1,17,18). The direct UV-irradiation of disulfides at $\lambda = 250 - 300$ nm can generate a pair of Cys thiyl radicals (CysS \cdot) (19–22) (reaction 1), which are reactive key intermediates in the photodegradation of peptides and proteins (23–26). Besides homolysis, CysS \cdot radicals are generated indirectly by the one electron reduction of disulfide bonds (reaction 2, equilibrium 3) (27,28), for instance by photo-induced electron transfer from Trp or Tyr (12–16). Furthermore, Cys thiolate (CysS $^-$), generated via equilibrium 3, can be photo-ionized to a CysS \cdot thiyl radical (reaction 4). In addition, thiyl radicals may be generated via thiol/thiolate oxidation through various radicals such as phenoxy, peroxy and alkoxy radicals, represented by XO \cdot in reaction 5 (29–31). Moreover, the one electron reduction of thioaldehydes (32) may also contribute as a minor secondary pathway to the formation of thiyl radicals (reaction sequence 6) (33).



CysS \cdot radicals can initiate a variety of different degradation pathways through disproportionation (reaction 7) (23), hydrogen abstraction (34–37) (reaction 8) or combination with

other peptide or protein radicals, representatively referred to as P \cdot (reaction 9) (16,34).



The disproportionation reaction 7 yields a free thiol and a thioaldehyde (23). The latter is an electrophile that can form dithiohemiacetals with thiols (23) or undergo hydrolysis to Ser semialdehyde (SerSA) (35). On the other hand, thiyl radicals can enter *intramolecular* 1,2- and 1,3-hydrogen transfer reactions and are capable of abstracting hydrogen atoms from amino acid residues as well as from the peptide backbone (31,33–37). Hydrogen abstraction from side chain residues may ultimately result in the formation of alcohols and carbonyls (38–41), while hydrogen abstraction from the Tyr hydroxyl group yields a phenoxy radical (31), and, potentially, a Tyr-Cys crosslink (25). The 1,3-hydrogen transfer within CysS \cdot yields a $\cdot\text{C}^\alpha$ radical from which the hydrogen sulfide radical HS \cdot can be eliminated to form dehydro-Ala (Dha) (23,33). In the presence of oxygen, $\cdot\text{C}^\alpha$ radicals can convert into peroxy radicals, which may initiate peptide bond cleavage by the diketo pathway (41). When converted to alkoxy radicals, peptide cleavage by the diamide pathway may occur (41).

We report here on the disulfide degradation pathways of hGH when photo-irradiated at $\lambda = 254$ nm or $\lambda > 295$ nm in aqueous solution, and provide mass spectrometric evidence for various new photo-degradation pathways, that include: the transformation of Cys to Gly, the formation of a vinyl ether between Ser-184 and a photoproduct of Cys-189, several novel cross-links, and two peptide cleavage reactions adjacent to Cys-53 leading to carbamate or an α -keto acid. The photo-irradiation experiments at $\lambda = 254$ nm were performed as proof-of-concept studies under conditions where the intensity of a single wavelength is well-defined. These conditions also mimic photolytic stress that protein pharmaceuticals may encounter during sterilization by UV-light, a proposed method for viral decontamination (6), or during chromatographic purification coupled to UV-detection (42,43). Photo-irradiation experiments at $\lambda > 295$ nm represent exposure to UV-B light that is not filtered by glass, i.e. conditions that may be encountered during transportation and storage, and exposure to fluorescent white light or sunlight. This article complements an earlier photodegradation study of hGH (44), in which we described an unusual cleavage between Glu-88 and Pro-89 in proximity to Trp-86 after photo-irradiation at $\lambda = 254$ nm, in addition to Met oxidation and new backbone cleavage reactions between Phe-1 and Pro-2.

In contrast to the pathways in aqueous solution reported here, a solid state photo-degradation study of the structurally

related bovine growth hormone revealed a Trp-dependent degradation mechanism, where an initial electron transfer from Trp to the disulfide bond, leads to the generation of CysS[•] radicals. After reaction with oxygen, the CysS[•] radicals eventually recombined to yield α -disulfoxide, thiosulfinate, and/or thiosulfonate (12).

EXPERIMENTAL SECTION

Materials

Human growth hormone (somatotropin, hGH) was provided as Nutropin AQ® formulations by Genentech, Inc. (South San Francisco, CA). The protein was separated from excipients by dialysis against water overnight with Slide-A-Lyzer Dialysis Cassettes of 3.5 K molecular weight cut off (MWCO) from Thermo Fisher Scientific Inc. (Rockford, IL). Alternatively, formulations were filtered and washed three times with water with Amicon Ultra-15 Ultracel - 10 k (10 kDa MWCO) centrifugal filters from EMD Millipore Corporation (Billerica, MA). Aliquots of ca. 0.1 ml were stored at -20°C and concentrations were measured by means of UV spectroscopy at 277 nm, where $A_{277} = 0.82\text{ cm}^{-1}$ (45). TPCK-treated sequence-grade trypsin was obtained from Promega (Madison, WI) (some digestions were performed with trypsin from Sigma-Aldrich (St. Louis, MO)), and ThioGlo® 1 was obtained from Millipore. All other chemicals were of the highest commercial grade available and obtained from Sigma (Saint Louis, MO) or Fisher (Pittsburgh, PA). Chemicals were used as received and all solutions were prepared with MilliporeQ-water.

Photo-Irradiation

Photo-irradiations were carried out in a Rayonet photo-reactor RPR-200 equipped with four 35 W low pressure mercury lamps (RPR-2537 Å) or four phosphor-coated low pressure mercury lamps (RPR-3000 Å). The RPR-2537 Å lamp has an emission $>80\%$ at $\lambda = 254\text{ nm}$ and the RPR-3000 Å lamp emits 95% of light between $\lambda = 265\text{--}340\text{ nm}$ ($\lambda_{\text{max}} = 300\text{ nm}$) (46). A rotating Rayonet RMA-500 Merry-Go-Around assured uniform light exposure of the samples that had a distance of 3.8 cm (1.5 in.) from the lamps. All equipment was from the Southern New England Ultra Violet Company (Branford, CT). Samples were placed in $13 \times 100\text{ mm}$ quartz glass tubes when irradiated at $\lambda = 254\text{ nm}$ or in equally sized borosilicate glass (akin to Pyrex) tubes to cut off light below 295 nm when irradiated with RPR-3000 Å lamps. The light intensity reading orthogonal to the lamps was 210 W/m^2 when 16 RPR-2537 Å lamps were employed at the distance of 1.5 in. (46). Hence, we calculate a light intensity of 52.5 W/m^2 for 4 lamps, and photo-

irradiations of 5 min correspond to ca. 4.4 Wh/m^2 . In contrast, the current ICH guidelines for photostability testing require 200 Wh/m^2 (47). However, we note that the ICH guideline makes use of a broad irradiation spectrum between 320 and 400 nm (47), whereas our experiments at 254 nm used light at a specific wavelength. Based on previous actinometry measurements, we calculate that samples were subjected to a total of 4.3×10^{-6} einstein (mol photons) when irradiated for 5 min with 4 RPR-2537 Å lamps. Due to the broad emission spectrum of the RPR-3000 Å lamps actinometry was not performed; the spectral distribution of irradiance density of the lamps is published by the manufacturer (46).

Preparation of Samples

Samples for irradiation had a volume of 400 μL , contained 10 μM (0.22 mg/ml) hGH and were buffered with 0.1 M phosphate at pH 7.4. After irradiation, samples were transferred to 2 ml centrifuge vials. Crystalline guanidine hydrochloride was added for a final concentration of 5 M. A 100-fold excess of N-ethylmaleimide (NEM) was added and the pH was adjusted to ca. 7.4 with 0.1 M tribasic sodium phosphate. After 10 min incubation at 37°C , hGH was precipitated with 1.4 ml 0.5 M HClO_4 and centrifuged at 14,000 g for 10 min. The resulting pellets were washed twice with water. Thereafter, tryptic digestion (trypsin/protein = 1:50) was performed in 100 μL aqueous solution, buffered at pH 7.8 with 0.1 M NH_4HCO_3 . After incubation at 37°C for 8 h, the digests were stored at -20°C prior to analysis.

Preparation of the Samples for Time-Dependent Analysis of the Photoproducts

hGH samples were reconstituted in 100 μL of NH_4HCO_3 buffer (50 mM, pH 7.5). The disulfide bonds were reduced by the addition of 50 μL of 5 mM stock solution of bis(2-mercaptoethyl)sulfone (BMS) in acetonitrile (ACN), followed by incubation at 45°C for 30 min. The reduced cysteine residues were alkylated by the addition of 50 μL of 25 mM iodoacetamide (IAA) in NH_4HCO_3 buffer (50 mM, pH 7.4), followed by incubation for 2 h at 37°C . After 2 h incubation at 37°C , hGH was precipitated with 700 μL of 0.5 M HClO_4 and centrifuged at 14,000 g for 10 min. The resulting pellet was washed twice with milliQ water. Thereafter, the pellet was reconstituted in 200 μL of NH_4HCO_3 buffer (50 mM, pH 8). 5 μg of trypsin (protein/trypsin = 40) were added to each sample (we noted, that digestions performed with porcine pancreas trypsin obtained from Sigma-Aldrich revealed some chymotryptic cleavage sites). After overnight incubation at 37°C , the proteolytic digests were purified using Amicon ultra-0.5 centrifugal devices equipped with 10 kDa NMWL membranes to separate undigested protein and trypsin from the proteolytic peptides.

Analysis on a SYNAPT-G2 Mass Spectrometer

For HPLC-MS1 analysis samples were analyzed on an Acquity UPLC® system (Waters Corp., Milford, MA), equipped with a Vydac 218MS™ capillary column (25 cm × 500 μm C18, 5 μm) from Grace (Deerfield, IL) and connected to a Synapt G2 mass spectrometer (Waters Corp., Milford, MA). 10 μl of tryptic digests were eluted with a 30 min linear gradient of 10–60% (v/v) ACN in aqueous formic acid (0.06%, v/v), followed by a second linear gradient of ACN in aqueous formic acid (0.06%, v/v) to 80% (v/v) within 10 min. The flow rate was set to 20 μl/min. All lenses in the G2 mass spectrometer were optimized on the $[M + 2H]^{2+}$ ion from the $[Glu]^{1}$ -fibrinopeptide for maximum resolution. The cone voltage was 45 V and Ar was admitted to the collision cell. The spectra were acquired between 50–2000 amu (amu = atomic mass unit) and the data were accumulated for 2 s per cycle. Analysis of raw data files was carried out with the MassLynx™ Software (Waters Corp., Milford, MA).

Analysis on an LTQ-FT-ICR Mass Spectrometer

The hybrid linear quadrupole ion trap Fourier transform-ion cyclotron resonance (LTQ-FT-ICR) mass spectrometer from ThermoFinnigan, Bremen, Germany was operated as described. (48) Liquid chromatography was carried out with an LC Packings Ultimate Chromatograph (Dionex, Sunnyvale, CA) system coupled to the same Vydac column (25 cm × 1 mm C18, 3.5 μm). MS2 spectra were recorded based on MS survey scans; MS2 and MS3 spectra of selected ions were recorded exclusively in separate runs for optimal spectrum quality. Raw data files were analyzed with the Xcalibur™ software package (ThermoFinnigan, Bremen, Germany). The program ReAdW version 4.3.1 was used to generate mzXML files for analysis with the MassMatrix program (49).

Analysis on an In-house Packed 75 cm C18 Nano-column Coupled to a Xevo-G2 Mass Spectrometer

We have constructed an ultra-high pressure chromatography system based on slight modifications of a published design (50). This chromatography system was equipped with an in-house prepared C18 nano-column (75 cm × 0.75 μm), packed with particles supplied by Waters Corporation (Charge Surface Hybrid, CSH™). The analytes were eluted through the column at a flow rate of 0.25 μL/min at a pressure of 34,000 psi. The mobile phases consisted of water/acetonitrile/formic acid at a ratio of 99%, 1%, 0.08% (v:v:v) for solvent A and a ratio of 1%, 99%, 0.06% (v:v:v) for solvent B. A linear gradient, starting with 7% A and changing A by 0.15%/min over 250 min was prepared using a NanoAcquity ultra-high

performance liquid chromatography (nanoAcquity-UPLC) system (Waters Corporation, Milford, MA), and stored in a 200 μL loop (50) prior to be pushed through the analytical column. More details about the chromatography system will be reported elsewhere. The chromatographic system was coupled to a Waters Xevo-G2 (Waters Corp., Milford, MA) mass spectrometer operating in the positive mode. A nanoflow gas pressure was set to 0.2 bar, with a cone gas flow set to 4 L/h and a source temperature of 100°C. The capillary voltage and cone voltage were set to 2800 V and 35 V, respectively. The Xevo-G2 acquisition rate was set to 0.5 s with a 0.0 s inter-scan delay. Ar was employed as the collision gas. The instrument was operated in the MSE mode. The instrument was operated with the first resolving quadrupole in a wide pass mode with the collision cell operating with different alternating energies. To acquire the non-fragmented MS1 spectrum the collision cell was operated at 5 eV. The fragmented MS1 ion spectra were acquired by ramping the collision cell energies between 15 eV and 45 eV. The data were collected into separate data channels. All analyses were acquired using the lockspray to ensure mass accuracy and reproducibility; $[Glu]^{1}$ -fibrinopeptide B was used as the lock mass (m/z 785.8426, doubly charged) at a concentration of 2 pmol/μL and flow rate of 1 μL/min. Data were collected in centroid mode, the lockspray frequency was set to 5 s, and data were averaged over 10 scans.

Estimation of the Yields of Degradation Products

We estimated the relative yields of the detected degradation products through the peak areas in the extracted ion chromatograms of the most abundant ions of the respective tryptic peptides. Since signal intensity strongly depends on the molecular weight and chemical structure of an ion, we only compared the signal intensities of products to signal intensities of the native, unmodified tryptic peptides. These are presented in Tables I and III. The relative abundances of the cross-links reported in Table II were estimated by comparing signal intensities of all detected cross-links, which, however, resulted in potentially large errors. Due to the inherent uncertainty of uncalibrated relative quantitation, relative abundances are only estimated and products are described as major (++) , minor (+; one order of magnitude lower signal intensity compared to ++) or as trace (t), when signals were below the quantitation limit. The loss of disulfide-containing tryptic fragments was calculated based on peak areas, and referenced to the more photolysis-resistant fragments T12 and T13 (LEDGSPR and TGQIFK) as internal standards. Yields of cross-links formed between T6 - T16 and T20 - T21 were estimated by dividing the peak area of the new cross-link by the peak area of the respective native disulfide in the control sample, corrected for concentration differences with T12 and T13 as internal standards.

Table 1 Amino Acid Modifications Observed After Irradiation at $\lambda = 254$ or $\lambda > 295$ nm and Subsequent Derivatization with NEM, Tentatively Assigned by MS and MS² Analysis

Peptide/Amino acid	Product	Tentative modification	m/z ^a	Abundance ^{b,c}		Figure ^d
				254 nm	>295 nm	
T6/C ⁵³	1	Cys-NEM	1371.15(d)	++	++	S11
T6/C ⁵³ ,F ⁵⁴	2	Cys thioaldehyde + dehydro-F ⁵⁴ (crosslink possible, product 48)	1306.61(d)	++	+	S39
T6/C ⁵³	3	Cys-NEM -2 Da	1370.65(d)	+	+	S49
T6/C ⁵³ ,L ⁵² or F ⁵⁴	4	Dha + dehydro-L ⁵² or -F ⁵⁴	1290.62(d)	t	t	S38
T6/C ⁵³	5	S-sulfocysteine (RSSO ₃ H)	1348.60	t	t	S61
T16/C ¹⁶⁵	6	Cys-NEM	637.31(d)	++	++	S12
T16/C ¹⁶⁵	7^e	Cys thioaldehyde	573.77(d)	+	+	S19
T16/C ¹⁶⁵	8	Cys sulfinic acid	582.40(d)	+	+	S59
T16/C ¹⁶⁵	9	Cys sulfonic acid	1196.55(s)	+	+	S56
T16/C ¹⁶⁵	10	Dha	557.79(d)	+ ^c	+ ^c	S15
T16/C ¹⁶⁵	11	Ala	1116.58(s)	+	+	S52
T16/C ¹⁶⁵	12	Gly	551.79(d)	+	+	1
T16/C ¹⁶⁵	13	SerSA	565.78(d)	+	+	S21
T16/C ¹⁶⁵	14	Ser	566.79(d)	t	+	S54
T16/C ¹⁶⁵ ,F ¹⁶⁶ ,R ¹⁶⁷	15	Cys thioaldehyde + dehydro F ¹⁶⁶ /R ¹⁶⁷ (crosslink possible, please see product 47 in Table II)	572.77(d)	t	t	S40
T16-T17/C ¹⁶⁵ ,R ¹⁶⁷ or K ¹⁶⁸	16	Cys thioaldehyde + dehydro-R ¹⁶⁷ or -K ¹⁶⁸	636.81(d)	t	t	3
T20/C ¹⁸²	17	Cys-NEM	743.39(s)	++	++	S13
T20/C ¹⁸²	18	Ala	586.37(s)	t	t	S53
T20/C ¹⁸²	19	Cys sulfonic acid	666.32(s)	+	+	S57
T20/C ¹⁸²	20	Dha	584.35(s)	+	+	S16
T20/C ¹⁸²	21	Gly	572.35 (s)	+	+	S58
T20/C ¹⁸² ,R ¹⁸³	22^e	Cys thioaldehyde + dehydro-R ¹⁸³	614.31(s)	+	+	S60
T20/C ¹⁸²	23	Cys-NEM -2 Da	741.37(s)	t	t	S50
T21/C ¹⁸⁹	24	Cys-NEM	910.36(s)	++	++	S14
T21/C ¹⁸⁹	25	Dha	751.33(s)	+ ^c	+ ^c	S17
T21/C ¹⁸⁹ ,F ¹⁹¹	26	Cys thioaldehyde + dehydro-F ¹⁹¹	781.30(s)	+	+	2
T21/C ¹⁸⁹	27	Cys sulfinic acid	817.30(s)	+	t	S59
T21/C ¹⁸⁹	28^e	Cys thioaldehyde	783.30(s)	t	t	S20
T21/C ¹⁸⁹	29	Gly	739.33(s)	t	t	S24
T21/C ¹⁸⁹	30	SerSA	767.32(s)	t	t	S23
T21/C ¹⁸⁹	31	Ser	769.34(s)	t	t	S22
T21/C ¹⁸⁹	32	Cys-NEM -2 Da	908.35(s)	t	t	S51
T9M ⁸⁶	33	Gly	963.57(d)	t	t	S18

^a Charge state of the ion is given as (s) and (d) for singly and doubly charged states, respectively

^b Abundance is given as ++ for major products, as + for minor products that showed one order of magnitude lower signal intensities, and as a "t" for trace amounts

^c If modifications were also found in control samples that were not irradiated, the designator "c" is added. Irradiation products obtained with $\lambda = 254$ nm and $\lambda > 295$ nm were evaluated separately and compared to modifications localized within the same tryptic fragment

^d Figures S11-S63 are available in the Supplementary Material

^e A loss of 44 Da from the parent ion was observed in the MS² spectrum. The latter was likely due to a decarboxylation reaction occurring during the fragmentation of the peptide ion (80). We observed this neutral loss only when a Cys residue was transformed into a thioaldehyde

The yields of free thiols were measured by derivatization with ThioGlo® 1 (51). Briefly, to irradiated samples 400 μ l of 6 M guanidine hydrochloride were added and the pH was

adjusted to 7 with 0.1 M Na₃PO₄. ThioGlo® 1 reagent (2 mM in ACN) was added for a final concentration of 20 μ M and the mixture was incubated for 30 min at room

Table II Crosslinks Observed After Irradiation at $\lambda = 254$ or $\lambda > 295$ nm and Derivatization with NEM

Peptide/amino acids ^a	Product	Tentative crosslink	m/z^b	Abundance ^{c,d}		Figure ^e
				254 nm	>295 nm	
T20-T21/C ¹⁸² -C ¹⁸⁹	34	dithiohemiacetal	763.34(d)	++	++	S31
T20-T21/C ¹⁸² -C ¹⁸⁹	35	vinyl thioether	683.82(d)	++	++	S32
T20-T21/C ¹⁸² -C ¹⁸⁹	36	thioether	684.83(d)	++	++	S34
T20-T21/C ¹⁸² -C ¹⁸⁹	37	divinyl disulfide	698.8(d)	+	t	S30
T21/S ¹⁸⁴ -C ¹⁸⁹	38	vinyl ether	749.31(d)	+	t	4, 5
T6-T16/C ⁵³ -C ¹⁶⁵	39	vinyl thioether	1243.28(t)	t	t	S33
T6-T16/C ⁵³ -C ¹⁶⁵	40	vinyl disulfide	1253.91(t)	+	t	S28
T16-T21/C ¹⁶⁵ -C ¹⁸⁹	41	vinyl disulfide	849.39(d)	+	t	S29
T21/C ¹⁸⁹ -C ¹⁸⁹	42	disulfide	784.3(d)	++	++	S27
T6-T20/C ⁵³ -C ¹⁸²	43	disulfide	808.64(q)	++	+	S25
T16-T21/C ¹⁶⁵ -C ¹⁸⁹	44	disulfide	965.93(d)	++ ^c	+ ^c	S26
T16/C ¹⁶⁵ -Y ¹⁶⁴	45	-36 Da mass shift	556.79(d)	+	t	6, 7
T16/C ¹⁶⁰ -Y ¹⁶⁴	46	-36 Da mass shift	556.79(d)	+	t	6,7
T16-T17/C ¹⁶⁵ -Y ¹⁶⁴	45	-36 Da mass shift	620.94(d)	t	t	S37
T16/C ¹⁶⁵ -F ¹⁶⁶	47	-4 Da mass shift or Product 15	572.77(d)	t	t	S40
T6/C ⁵³ -F ⁵⁴	48	-4 Da mass shift or Product 2	1306.61(d)	++	+	S39
T9-T16/W ⁸⁶ -C ¹⁶⁵	49	thioether	1067.58(t)	t	t	S41
T9-T16/W ⁸⁶ -C ¹⁶⁵	50	indole-C β '-C α '	1056.92(t)	t	t	S42
T9-T14/W ⁸⁶ -Y ¹⁴³	51	indole-phenol	893.50(t)	t	t	S36
T10-T14/Y ¹¹¹ -Y ¹⁴³	52	dityrosine	962.48(t)	t	t	S35

^a Location of crosslinked amino acids are given by the tryptic fragments and amino acids, e.g. T20/C¹⁸²-T21/C¹⁸⁹: crosslink between Cys-182 in tryptic fragment T20 and Cys-189 in tryptic fragment T21

^b The charge state of the ion is given in parenthesis as s, d, t, q for singly, doubly and triply charged states, respectively

^c If modifications were also found in control samples that were not irradiated, the designator "c" is added

^d Abundance is given as ++ for major products, as + for minor products that showed one order of magnitude lower signal intensities, and as a "t" for trace amounts. Samples irradiated at $\lambda = 254$ and $\lambda > 295$ nm were evaluated separately

^e Figures S11-S63 are available in the Supplementary Material

temperature. For calibration, non-irradiated samples were reduced with 0.1 M NaBH₄ in 400 μ l guanidine chloride (6 M) at pH 9 for 15 min at 37°C. The remaining NaBH₄ was quenched by lowering the pH to 6.0 with 0.2 M NaH₂PO₃. Thereafter, the pH was adjusted to 7 with 0.1 M Na₃PO₄ and the volume was adjusted to 800 μ l with water. ThioGlo® 1 was added for a final concentration of 20 μ M. After incubation for 30 min at room temperature, the fluorescence was measured (Ex: $\lambda = 379$ nm, Em: $\lambda = 513$ nm). Fluorescence readings were corrected for background fluorescence by subtracting the fluorescence of non-irradiated, non-reduced samples that were treated with ThioGlo® 1.

Data Analysis

Targeted data analysis for known disulfide degradation products was performed by the MassMatrix program (49). Non-targeted data analysis was performed by analyzing strong newly formed peaks manually.

RESULTS

We photo-irradiated hGH at $\lambda = 254$ nm and $\lambda > 295$ nm for typically 5 min and 1 h, respectively, and thereafter free thiols were alkylated with NEM. The mass spectrometric analysis of tryptic digests (Tables I, II, and III, Figs. 1, 2, 3, 4, 5, 6, 7, 8, and 9 and Supplementary Information, Figs. S11-S63) showed that such irradiation conditions degraded the disulfide-containing tryptic peptides by ca. 80% ($\lambda = 254$ nm) and 20% ($\lambda > 295$ nm), respectively. Chromatograms of tryptic maps comparing control and irradiated hGH under both photo-irradiation conditions are displayed in Figs. S64 and S65. After the irradiation at both wavelengths we observed an increase of background signals in the total ion count chromatograms (TIC) during HPLC-MS analysis, very similar to that observed when hGH was subjected to oxygen centered radicals derived from AAPH (52), likely indicating the formation of a variety of products at relatively low yields.

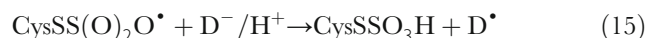
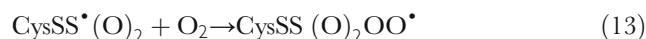
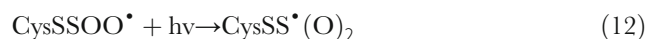
In Tables I, II, and III, which summarize the photochemical products, the majority of structures can be assigned by MS¹, MS² and/or MS³ analysis and by comparison to analogous products, which we characterized for the photo-degradation of a series of model peptides (23). Nevertheless, we must consider the structural assignments tentative as we could not fractionate sufficient quantities for complementary NMR analysis. Tryptic digests were screened for known disulfide degradation products by HPLC-MS analysis and non-targeted screening was performed on prominent newly formed peaks after photo-irradiation. The detected modifications are summarized in Tables I, II, and III as single amino acid modifications, cross-links and cleavage products, respectively. In Tables I, II, and III we have grouped all the different modifications of an individual amino acid in clusters, according to the position of the original amino acid in the hGH sequence and its respective tryptic fragment (referred to as T). The corresponding mass spectra in support of the product structure(s) are referenced in the last columns of the Tables. Figures 1, 2, 3, 4, 5, 6, 7, 8, 9, and 10 are presented in the manuscript while Figs. S11-S63 are located in the Supplementary Information.

Single Amino Acid Modifications on Individual Tryptic Peptides

The photo-degradation products with highest signal intensities observed for all originally Cys-containing peptides, except Cys⁵³ in T6, irradiated at $\lambda = 254$ nm, were the reduced Cys residues, subsequently alkylated with NEM (+125 Da) (Table I, products 1, 6, 17, and 24 containing Cys-NEM). The hydrolysis products of NEM (+143 Da), which can form during tryptic digestion (53), were detected only in low yields and are, therefore, not included in Table I. Analysis of irradiated protein samples with ThioGlo® 1 revealed that the ratio [Cys]:[0.5 cystine], i.e. a measure for the formation of reduced Cys per Cys residues present in the original disulfide bond, was ca. 0.3 after 5 min of irradiation at $\lambda = 254$ nm and ca. 0.08 after 1 h of irradiation at $\lambda > 295$ nm. Consistent with a disproportionation mechanism of CysS[•] radical pairs, (23) we also detected the formation of Cys thioaldehyde (2-amino-3-thioxopropanoic acid; MW_{Cys} - 2 Da) for two Cys residues (products 7 and 28), albeit at lower yields as compared to reduced Cys residues. Such lower yields of Cys thioaldehydes are expected based on their potential for hydrolysis to serine aldehyde (SerSA), or subsequent reactions of Cys thioaldehyde, and its tautomeric form, 2-amino-3-mercaptoacrylic acid, to form dithiohemiacetals, vinyl thioethers and other products (see below). In fact, the derivatization of photo-irradiated hGH with NEM yields NEM-adducts of 2-amino-3-mercaptoacrylic acid in tryptic fragments T6, T20 and T21 (products 3, 23 and 32).

Through 1,3-hydrogen transfer, CysS[•] radicals exist in equilibrium with [•]C^α radicals, which can subsequently eliminate HS[•] to yield Dha with a rate constant on the order of $5 \times 10^3 \text{ s}^{-1}$ (33). Consistent with such mechanism, we detected Dha formation for three Cys residues present in hGH (products 10, 20, and 25). We note, however, that some conversion of Cys¹⁶⁵ (T16) and Cys¹⁸⁹ (T21) to Dha is also detected in control samples, which may be the result of β -elimination during sample preparation for analysis.

We observed trace amounts of S-sulfocysteine (CysSSO₃H; product 5) in T6, likely originating from minor yields of Cys perthiyl radicals (CysSS[•]) generated through reaction 10 (reaction 10 is representatively shown for isolated cysteine). (54) Perthiyl radicals add oxygen, and a plausible (54) route to S-sulfocysteine is provided by reactions 11-15, where D⁻ represents a suitable electron donor, e.g. CysSH or CysS⁻ (in competition to reaction 15, the radical CysSS(O)₂O[•] can release SO₃ to yield CysS[•]) (54).



The addition of oxygen to CysS[•] (55,56) will ultimately lead to oxy acids. Consistent with the predominant formation of CysS[•] via reaction 1, we detect the formation of Cys sulfinic acid in T16 and T21 (products 8 and 27), and the formation of Cys sulfonic acid in T16 and T20 (products 9 and 19).

We detected the conversion of Cys to Ala for Cys¹⁶⁵ and Cys¹⁸² (products 11 and 18), consistent with earlier reports on the photolysis of isolated cystine (57–59). Mechanistically, Ala can be obtained through reduction of Dha by electrons generated via reaction 4 (35), consistent with the observation of Dha (products 10, 20 and 25; see above). However, an alternative route for Ala formation would be reduction of alanyl-C^β radicals generated via reaction 10.

The conversion of Cys to Gly, detected for Cys¹⁶⁵, Cys¹⁸² and Cys¹⁸⁹ (products 12, 21 and 29) represents an important novel modification. Figure 1 displays representative data for the MS/MS characterization of Gly originating from Cys¹⁶⁵ in the tryptic peptide T16. Mechanistically, the formation of Gly can be rationalized through 1,2-hydrogen transfer of an initial CysS[•] radical (33) (see Discussion). The latter mechanism also provides an entry for the formation of serine aldehyde (SerSA), detected in peptides T16 and T21 (products 13

Table III Peptide Cleavages Observed After Irradiation at $\lambda = 254$ or $\lambda > 295$ nm and Subsequent Derivatization with NEM

Peptide/amino acid	Product	Tentative cleavage fragments ^a	m/z ^b	Abundance ^c		Figure ^d
				254 nm	>295 nm	
T6/L ⁵²	53	YSFLQNPTQTS- <i>LCFSESIPTPSNR</i>	1184.55(s)	+	t	S44
	54	YSFLQNPTQTS(amide)- <i>LCFSESIPTPSNR</i>	1183.55(s)	t	t	S43
T6/C ⁵³	55	YSFLQNPTQTS(amide)- <i>CFSESIPTPSNR</i>	1296.55(s)	+	+	S45
	56	YSFLQNPTQTS(-31 Da)- <i>CFSESIPTPSNR</i>	1306.56(s)	+	+	9
	57	YSFLQNPTQTS(+26 Da)- <i>CFSESIPTPSNR</i>	1260.57(s)	+	t	8
	58	YSFLQNPTQTS(-19 Da)- <i>CFSESIPTPSNR</i>	1318.57(s)	t	t	S48
T16/C ¹⁶⁵	59	NYGLLY- <i>CFR</i>	742.39(s)	+	+	S47
	60	NYGLLY(amide)- <i>CFR</i>	741.39(s)	+	+	S46

^a Detected fragments are given in regular letters, chemical modifications of peptides at the cleavage site are indicated by mass changes in parenthesis, and the remaining peptide sequence of the original tryptic peptide is given in italic font

^b The charge state of the ion is given in parenthesis as s, d, for singly and doubly charged states, respectively

^c Abundance is given as ++ for major products, as + for minor products that showed one order of magnitude lower signal intensities, and as a "t" for trace amounts. Irradiation products with $\lambda = 254$ nm and $\lambda > 295$ nm were evaluated separately and only compared to fragments of the same precursor peptide

^d Figures S11-S63 are available in the Supplementary Material

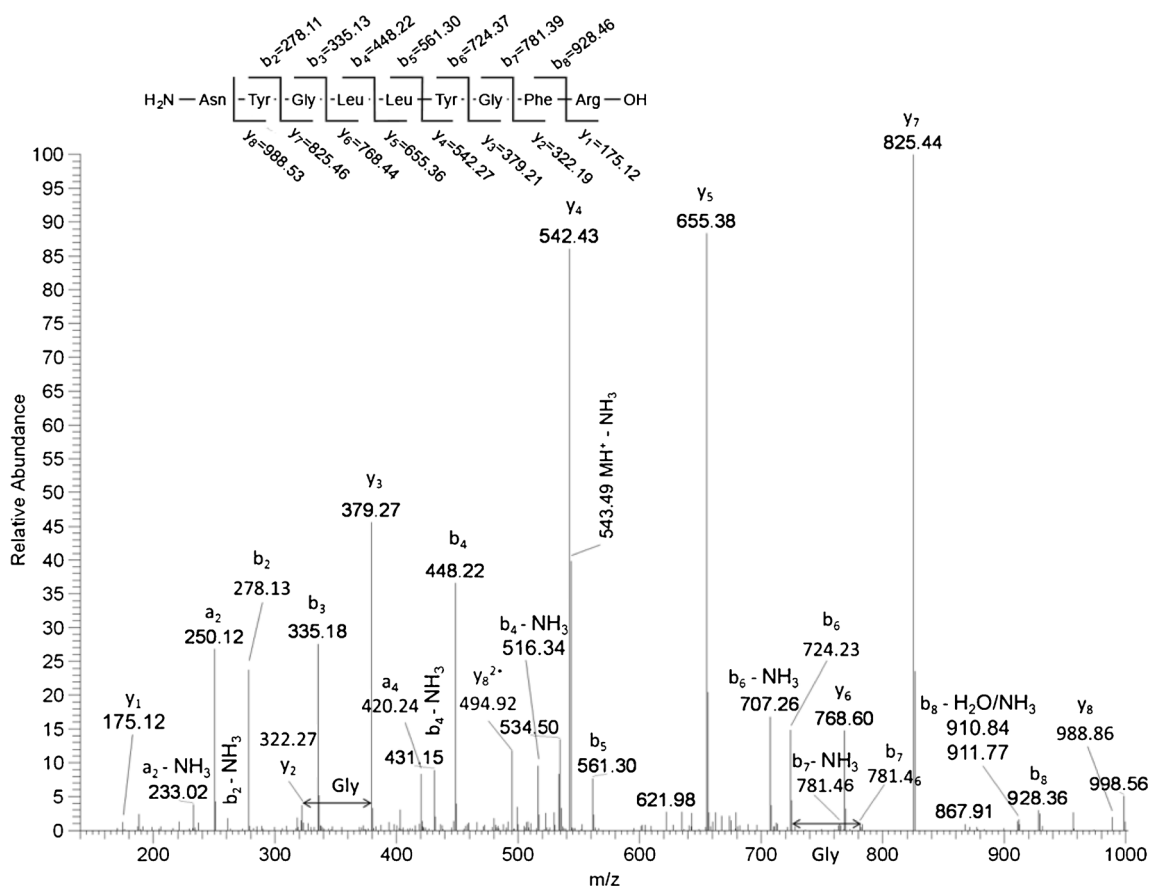


Fig. 1 MS² spectrum and tentative structure of the doubly charged precursor ion with m/z = 551.79 assigned to NYGLLYGFR and derived from T16 (NYGLLYCFR). The spectrum is in excellent agreement with the Cys-165 to Gly-165 transformation. The sample contained 10 μ M hGH in 0.4 ml phosphate (0.1 M, pH 7.4) and was photo-irradiated at $\lambda = 254$ nm for 10 min with four RPR-2537 Å lamps. After irradiation a 100-fold excess of NEM and crystalline guanidine for final concentration of 5 M was added; the pH was adjusted to ca. pH 7.4 with tribasic phosphate 0.1 M. After precipitation with 0.5 M HClO₄, and two washing steps with water, the protein pellets were resolubilized and digested. Tryptic peptides were analyzed by an LTQ-FTICR mass spectrometer.

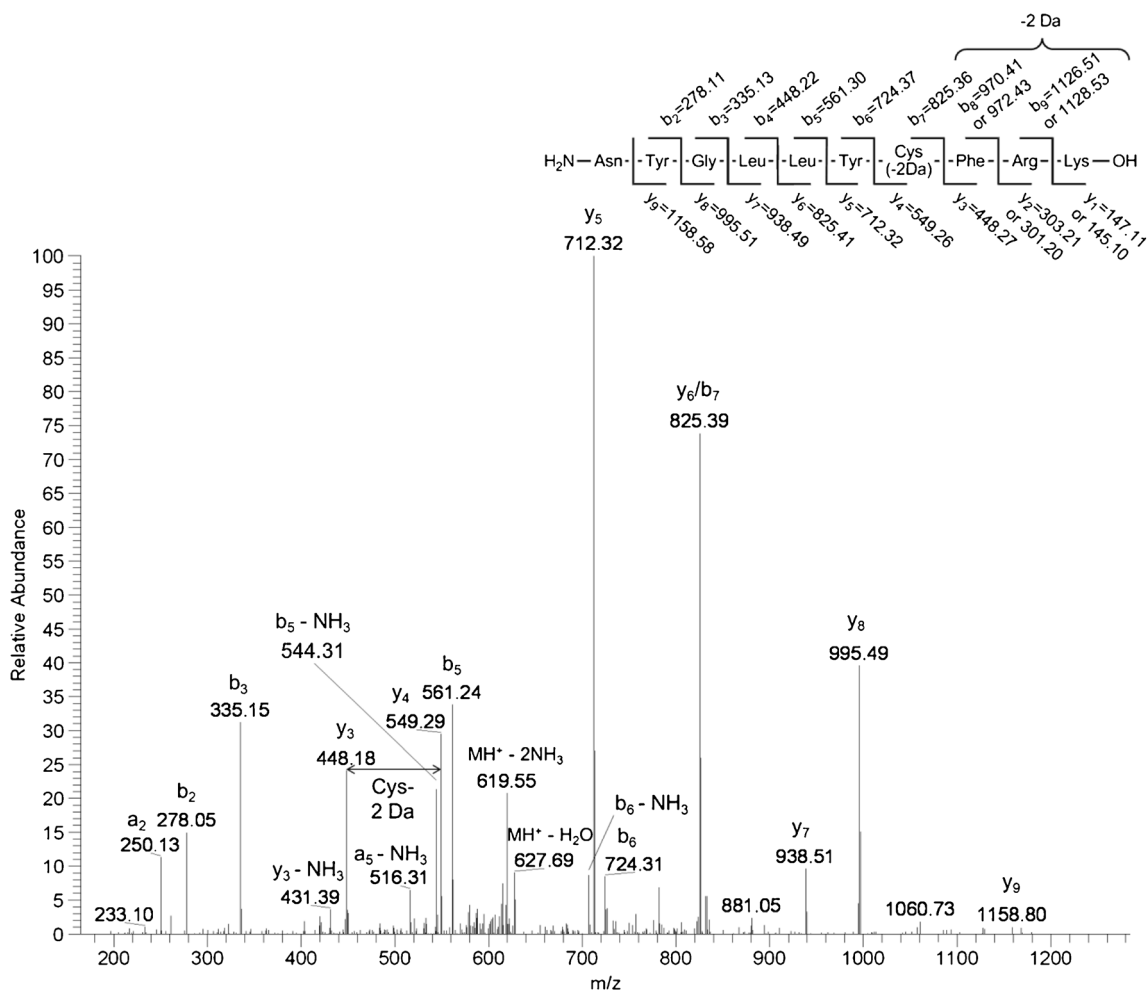


Fig. 2 MS² spectrum and tentative structure of the doubly charged precursor ion with $m/z = 636.82$ derived from T16-T17 (NYGLLYCFRK). The spectrum is in agreement with a dehydrogenation of Cys-165 to a thioaldehyde and a dehydrogenation of Phe-196, Arg-167 or Lys-168. Peaks with $m/z = 448.18$ and 549.29 are assigned to the y_3 and y_4 fragments which correspond to cleavage before and after Cys-165 thioaldehyde. Conditions as in Fig. 1.

and **30**). However, SerSA may also be formed through the hydrolysis of thioaldehydes, such as observed for peptides T16 and T21 in products **7** and **28** (see above), and through oxygen addition to alanyl-C^β radicals, followed by the Russell mechanism (60). Importantly, the Russell mechanism would also yield Ser, a product which was, in fact, observed in peptides T16 and T21 (products **14** and **31**).

An important pathway for peptide sequence modification is also the conversion of Trp to Gly (product **33**), detected for Trp⁸⁶ in peptide T9. Originally, we had reported such a modification for several Trp residues in monoclonal antibodies and model peptides, initiated through photo-induced electron transfer from Trp to a nearby disulfide bond (8).

Multiple Amino Acid Modifications on Individual Tryptic Peptides

We detected several products which contained multiple modified amino acids on individual tryptic peptides. These

products will be described in the following sections; however, for most of these products an unambiguous structural assignment was not possible as the mass spectrometry data would be consistent with several isobaric structures.

One modification of T6 displayed a mass shift of -4 Da (product **2**). This product showed the highest signal intensity of all T6-derived photo-degradation products. The MS/MS data are consistent with a loss of 2 Da from each Cys⁵³ and Phe⁵⁴, possibly indicating the formation of thioaldehyde (or its tautomer, 2-amino-3-mercaptoacrylic acid) and dehydrophenylalanine. However, we were unable to detect abundant b_{12} and y_{11} fragments, indicating that fragmentation between Cys⁵³ and Phe⁵⁴ may not be possible. This feature may indicate a cross-link generated from the original Cys⁵³ and Phe⁵⁴ residues, such as a vinyl thioether cross-link formed by reaction of 2-amino-3-mercaptoacrylic acid with dehydrophenylalanine (because of the cross-link nature of the latter, this potential structure is also listed as product **48** in Table II; see below). An additional modification of T6 displayed a mass shift of -36 Da (product **4**). The MS/MS data

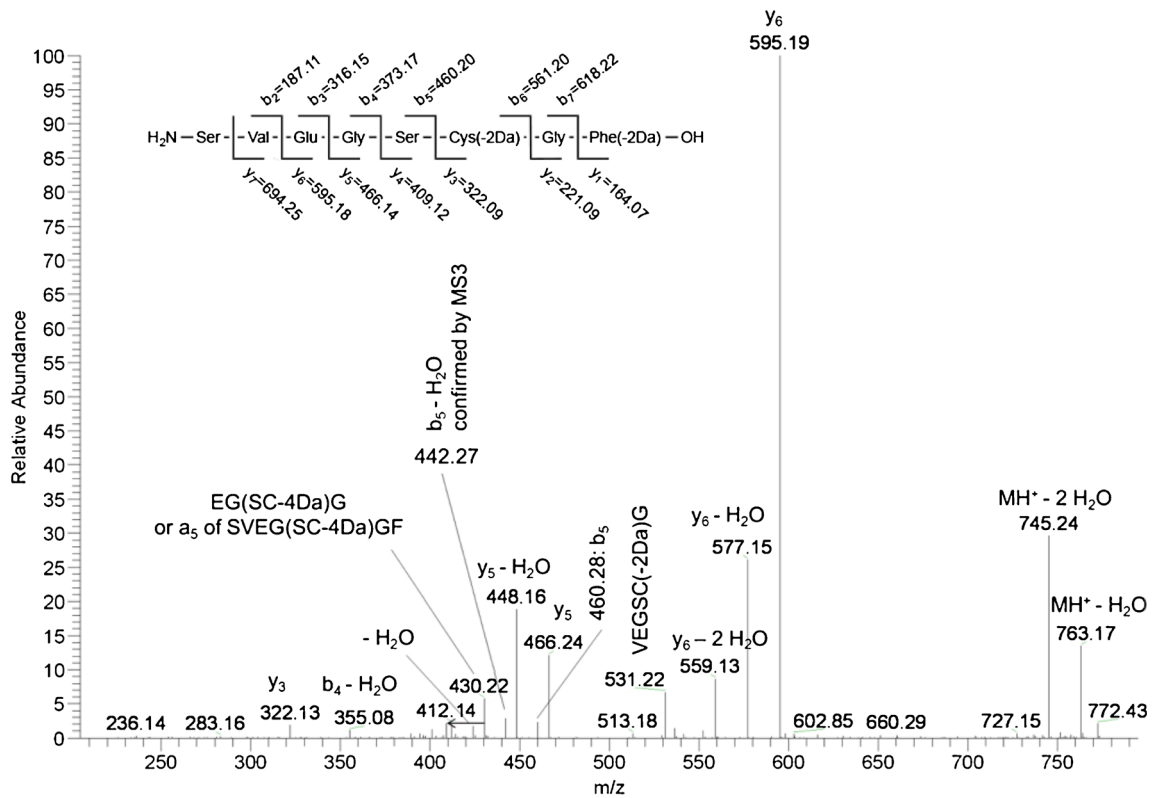


Fig. 3 MS² spectrum and tentative structure of the doubly charged precursor ion with $m/z = 781.28$ derived from T2I (SVEGSCGF). The spectrum is in agreement with a dehydrogenation of Cys-189 to a thioaldehyde and a dehydrogenation of Phe-191. Peaks with $m/z = 430.22$ and 412.14 could originate from a coeluting isobaric species that is characterized by a mass shift of -4 Da shared by Ser-188 and Cys-189. Conditions as in Fig. 1.

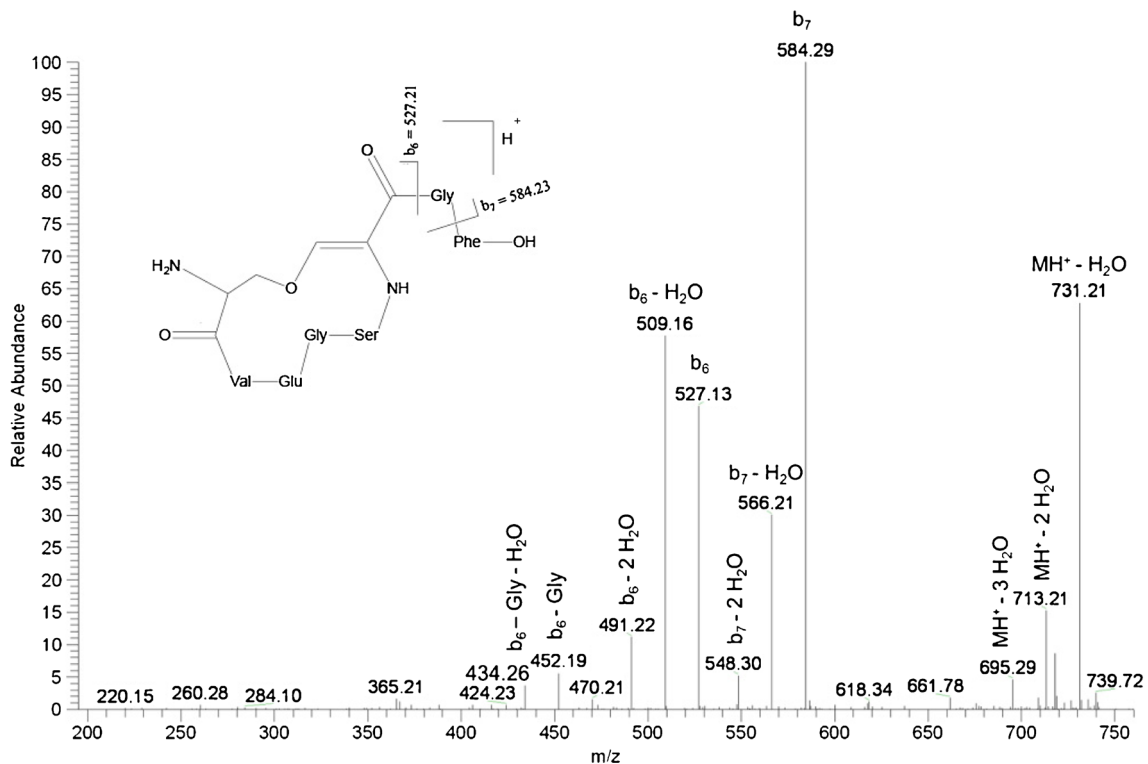


Fig. 4 MS² spectrum and tentative structure of the singly charged precursor ion with $m/z = 749.32$ derived from T2I (SVEGSCGF). The cyclic peptide structure exclusively leads to strong b₇ and b₆ fragments. Conditions as in Fig. 1.

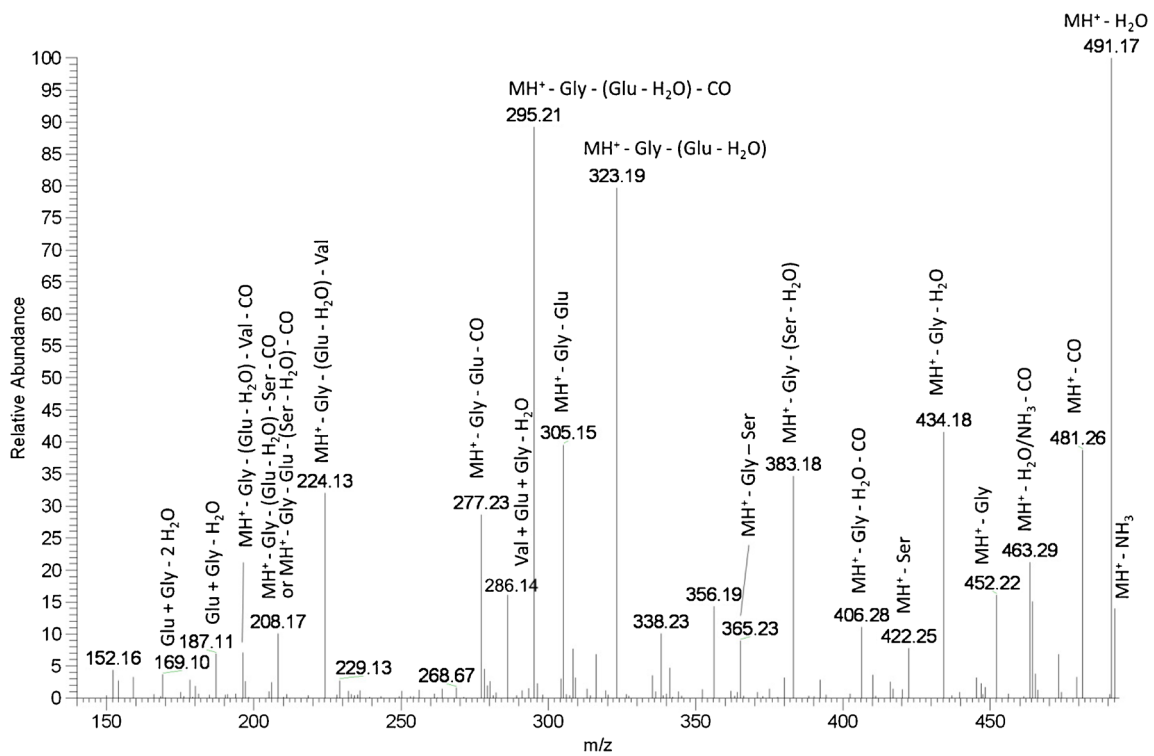


Fig. 5 MS³ spectrum of the singly charged ion with m/z 509.16 which is the b₆ - H₂O fragment of the precursor ion with m/z = 749.32 (Fig. 4). The fragmentation pattern used to assign peaks is displayed in Scheme 1. The sample was prepared as described in Fig. 1.

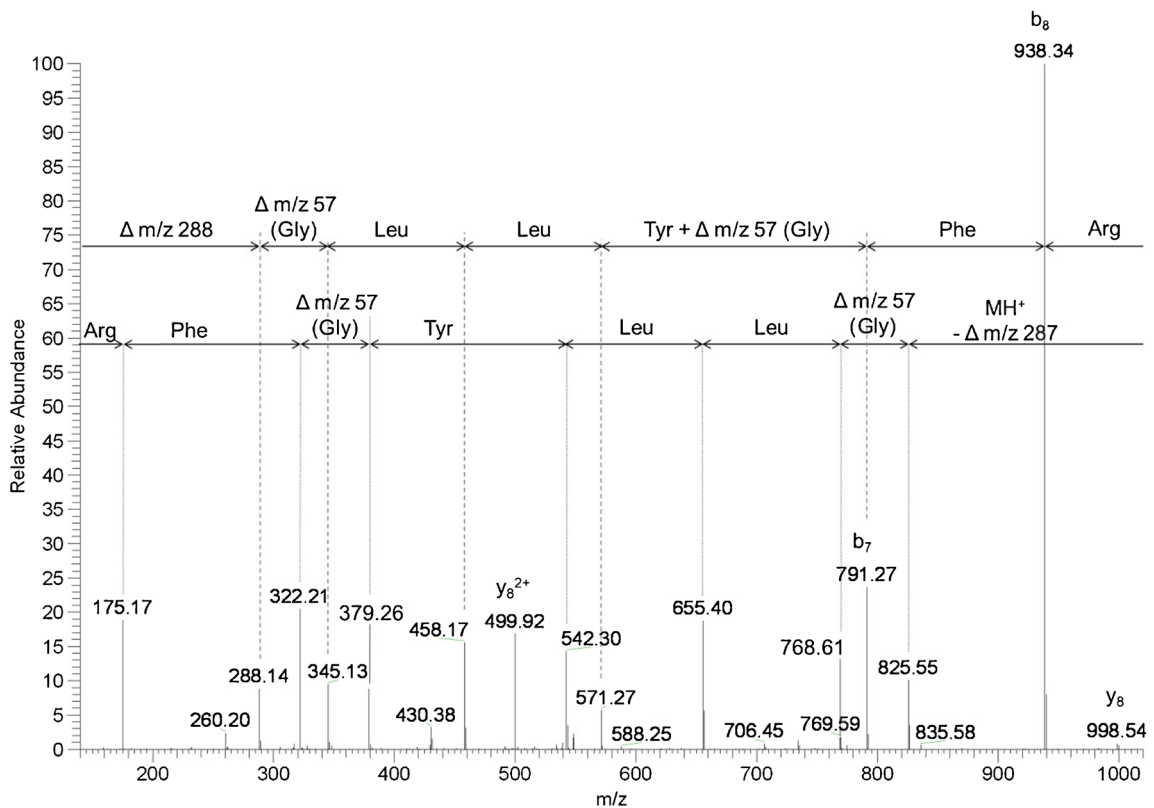
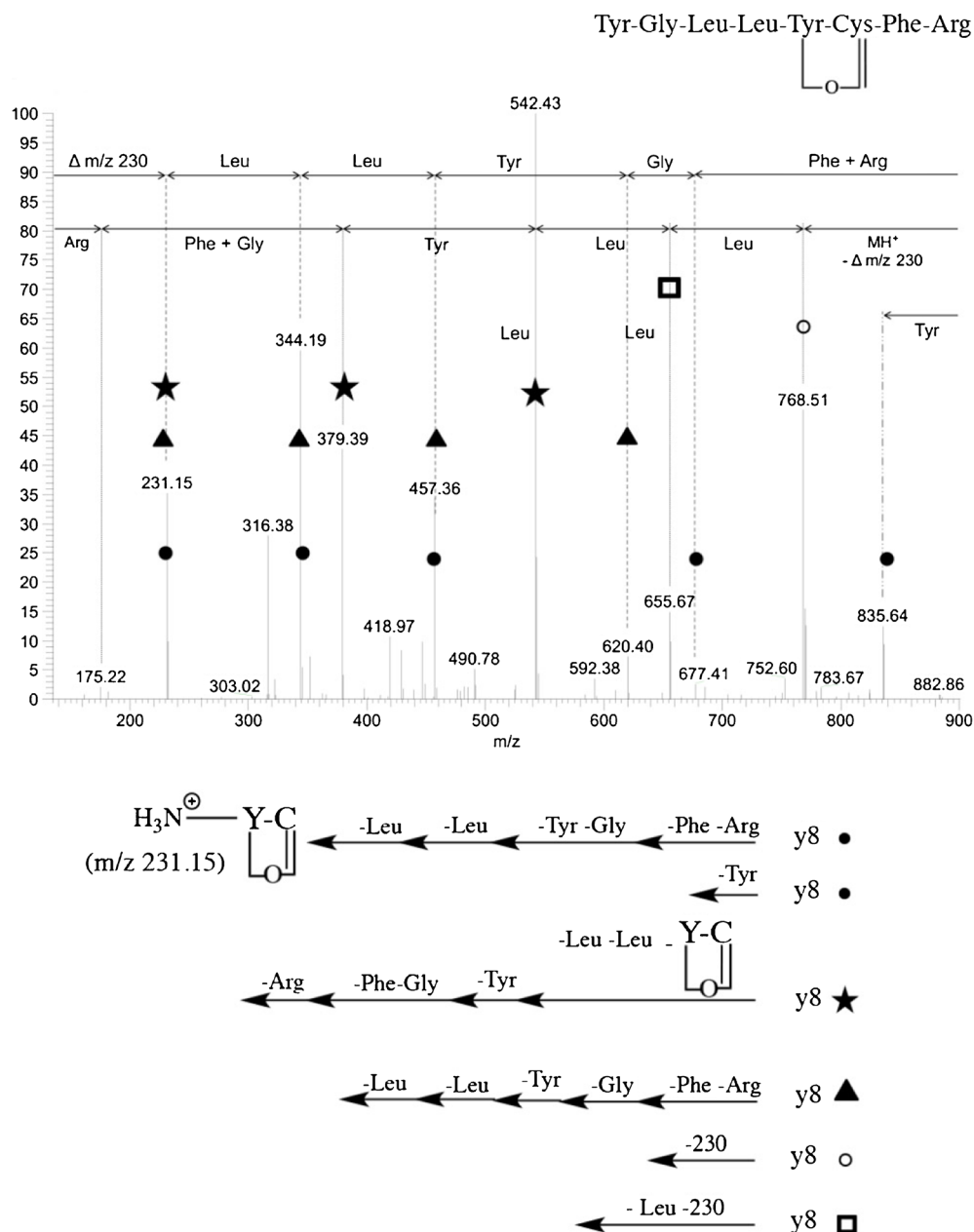


Fig. 6 MS² spectrum and tentative structure of the doubly charged precursor ion with m/z = 556.78 derived from T16 (NYGLLYCFR). The spectrum is in agreement with a linear peptide of the sequence NY(+10 Da)GLLGFR which is an unlike structure from a chemical viewpoint. Figure 7 shows the MS³ spectrum of y₈²⁺ that suggest a crosslinked Tyr-Cys derived structure modified by a mass shift of -36 Da.

Fig. 7 MS³ spectrum of the y_8^{2+} fragment ($m/z = 499.92$) derived from the doubly charged precursor ion with $m/z = 556.78$ (Fig. 5) which is a -36 Da modification of T16 (NYGLLYCFR). The spectrum would be in agreement with a structure that features the shown cross-link (referred to as structure **cY** in the text), characterized by a mass shift of -36 Da. Conditions as in Fig. 1.



are consistent with the conversion of Cys⁵³ to Dha and either Leu⁵² to dehydroleucine or Phe⁵⁴ to dehydrophenylalanine.

We detected a modification of T16 with a mass shift of -4 Da (product **15**). The MS/MS spectrum suggests that the modification is located on the subsequence Cys¹⁶⁵-Phe¹⁶⁶-Arg¹⁶⁷. However, the spectrum cannot discriminate between two separate modifications of -2 Da on two amino acids or a vinyl thioether cross-link between 2-amino-3-mercaptoacrylic acid derived from Cys¹⁶⁵ and either dehydrophenylalanine or dehydroarginine (hence, this product is also listed as product **47** in Table II).

An additional modification, on the tryptic peptide T16-T17 (containing one missed tryptic cleavage site), displayed a mass shift of -4 Da (product **16**). Here,

the MS/MS data clearly suggest the conversion of Cys¹⁶⁵ into thioaldehyde (or its tautomer, 2-amino-3-mercaptoacrylic acid) and an additional dehydroamino acid, either dehydrophenylalanine¹⁶⁶, dehydroarginine¹⁶⁷ or dehydrolysine¹⁶⁸ (Fig. 2).

We detected a modification of T20 that displayed a mass shift of -4 Da (product **22**). The MS2 spectrum suggests two modifications, the conversion of Cys¹⁸² into the respective thioaldehyde and of Arg¹⁸³ into dehydroarginine.

A product of the tryptic peptide T21 displayed a mass shift of -4 Da (product **26**). The spectrum displayed in Fig. 3 indicates that two isobaric species could be coeluting: *i*) a product where Cys¹⁸⁹ is converted into thioaldehyde (or its tautomer, 2-amino-3-mercaptoacrylic acid) and Phe¹⁹¹ is converted into

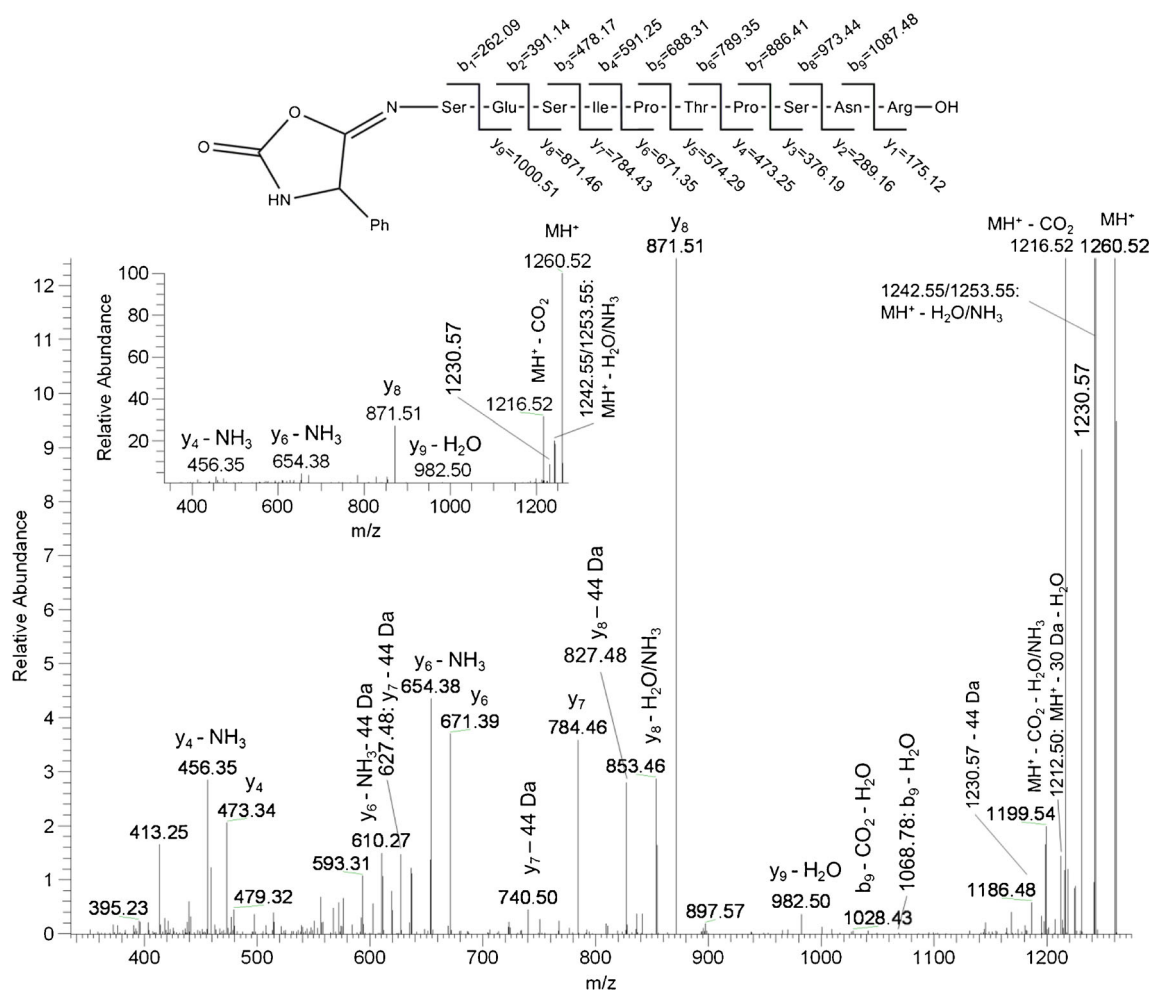


Fig. 8 Magnified and full (insert) MS² spectrum as well as tentative structure of the doubly charged precursor ion with $m/z = 1260.52$ derived from T6 (YSFLQNPQTSLCSFSESIPTSNR). The loss of CO₂ from MH⁺ is in agreement with a carbamate structure. The lack of the y₁₀ fragment of T6 but presence of the y₉ - H₂O fragment suggest the proposed cyclic structure. Conditions as in Fig. 1.

dehydrophenylalanine, and *ii*) a product with a vinyl thiohemiacetal crosslink between 2-amino-3-mercaptoacrylic acid generated from Cys¹⁸⁹ and SerSA generated from Ser¹⁸⁸.

Crosslinks

The photo-degradation of hGH led to the formation of various covalent cross-links, which are summarized in Table II and described in detail below. We detected a dithiohemiacetal crosslink (product **34**) between Cys¹⁸² and Cys¹⁸⁹ within tryptic peptides T20 and T21, alkylated with NEM (+125 Da mass shift relative to the disulfide). This crosslink was generated with an estimated yield of 2.5% when hGH was irradiated for 5 min at $\lambda = 254$ nm and an estimated yield of 1.5% when hGH was irradiated for 1 h at $\lambda > 295$ nm. Such dithiohemiacetal crosslinks have been characterized in detail by mass spectrometry and NMR for the photo-degradation of cystine-containing model peptides (23) but also observed during the photo-irradiation of insulin (25) and a monoclonal antibody (61). Mechanistically, they are likely generated

through the reaction of a Cys thiol with a thioaldehyde (though, technically, the combination of a Cys thiol radical with a Cys-derived α -mercaptoalkyl radical would provide an alternative route) (23). Another cross-link generated with significant yields was a vinyl thioether between photo-products generated from Cys¹⁸² and Cys¹⁸⁹ (product **35**) and between photo-products generated from Cys⁵³ and Cys¹⁶⁵ (product **39**). Product **35** was generated with an estimated yield of 3.9% when hGH was irradiated for 5 min at $\lambda = 254$ nm and a yield of 0.4% when hGH was irradiated for 1 h at $\lambda > 295$ nm while product **39** was only generated in trace amounts. Mechanistically, such vinyl thioether can form via at least two pathways: (i) the reaction of 2-amino-3-mercaptoacrylic acid with Dha, both of which have been detected for Cys¹⁸² and Cys¹⁸⁹ (Table I) (these vinyl thioethers can be resolved into various isomers on a 75 cm nano-column; see below), and (ii) the photochemical decomposition of dithiohemiacetal (23) (such as product **34**). The photochemical decomposition of dithiohemiacetal generates H₂S/HS⁻, which, during light exposure, can reduce the vinyl thioether

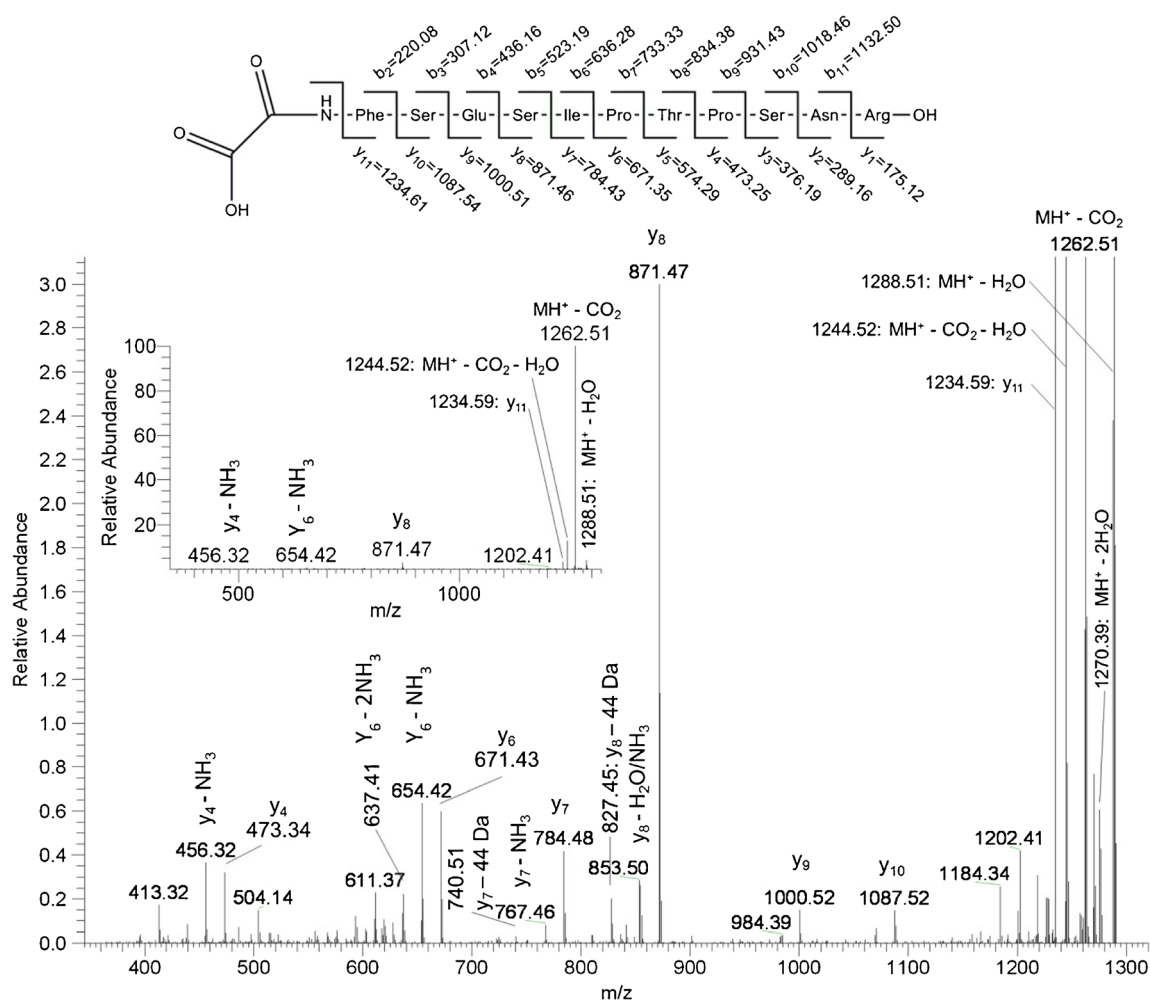


Fig. 9 Magnified and full (insert) MS² spectrum as well as the tentative structure of the doubly charged precursor ion with $m/z = 1306.58$ derived from T6 (YSFLQNPQTSLCFSEIPTPSNR). The y_{11} fragment gives evidence of a Cys⁵³-derived modification of $m/z = 71.97$ on the N-terminus of the cleavage fragment. Conditions as in Fig. 1.

further to the thioether (23). Not surprisingly, thioether crosslinks between Cys¹⁸² and Cys¹⁸⁹ were detected as major products (product **36**), with an estimated yield of 2.2% when hGH was irradiated for 5 min at $\lambda = 254$ nm and a yield of 1.2% when hGH was irradiated for 1 h at $\lambda > 295$ nm. The formation of such thioether can have a significant impact on the activity of hGH (62). Interestingly, a vinyl disulfide (of minor yield) was detected in place of the original disulfides in the tryptic peptide T6-T16 (product **40**; originating from Cys⁵³ and Cys¹⁶⁵). In addition, traces of a vinyl disulfide were generated from Cys¹⁶⁵ and Cys¹⁸⁹ (product **41**), and traces of a divinyl disulfide were generated between Cys¹⁸² and Cys¹⁸⁹ (product **37**).

MS² and MS³ spectra (Figs. 4 and 5) are consistent with a vinyl ether crosslink between Ser-184 and a reaction product from Cys-189 in T21 (product **38**). A tentative structure of product **38** is displayed in the insert in Fig. 4. The MS² spectrum of the precursor ion with m/z 749.31 (Fig. 4) displays dominant b_6 and b_7 fragments, which indicate selective fragmentation exclusively N-terminal of Gly-190 as well as

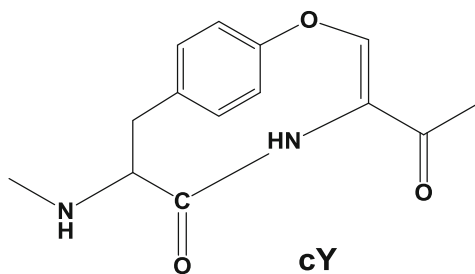
between Gly-190 and Phe-191. This strongly suggests a cyclic structure connecting reaction products of Ser-184 and Cys-189. In comparison, the native peptide, SVEGSCGF, alkylated with NEM, shows highly abundant y_5 and y_6 fragments (cleavages between Val-185, Glu-186 and Gly-187). Further evidence for a crosslink between products of Ser-184 and Cys-189 is obtained by examining the MS³ spectrum of the dehydrated b_6 ion (b_6 -H₂O), a putative cyclic peptide (Fig. 5). A tentative mechanism for the fragmentation of product **38** during MS² and MS³ analysis (of the b_6 -H₂O fragment) is displayed in Scheme 1. The prime peaks in the MS³ spectrum can be well assigned by the following fragmentation sequence: First, small neutral molecules such as H₂O and CO are lost, or alternatively, the cyclic structure is ruptured followed by the elimination of Gly¹⁸⁷ to give the product ion with $m/z = 450.2$. Second, either Ser¹⁸⁸, or Glu¹⁸⁶ are lost. The sites for dehydration of the precursor ion b_6 - H₂O are either Ser¹⁸⁸ or Glu¹⁸⁶ and, hence, fragmentation patterns of both the native and dehydrated amino acids Ser and Glu are observed. The loss of Glu¹⁸⁶ is followed by that of Val¹⁸⁵ which

leads to the products ions with $m/z = 224.02$ and $m/z = 206.06$.

We observed a total of three disulfide scrambling products (products **42-44**), rationalized by the photolytic formation of Cys (products **1**, **6**, **17** and **24**; see above) followed by disulfide exchange processes during photo-irradiation (note, that NEM was added after photo-irradiation minimizing disulfide exchange during sample preparation for analysis). Importantly, one of the new disulfides observed was a symmetric disulfide (product **42**), i.e. formed between identical peptides on different hGH molecules.

We detected a modification of T16, generated through the loss of 36 Da (original sequence: NYGLLYCFR) (product **45**). Product **45** displays complex MS2 and MS3 spectra (Figs. 6 and 7). The MS2 spectrum (Fig. 6) of the doubly charged molecular ion (m/z 556.78) shows a series of distinct fragmentation patterns. We observe the ions y_1^+ (m/z 175.17) and y_2^+ (m/z 322.21), indicating the cleavage of unmodified Arg and Arg-Phe from the C-terminus. We also observe the ions b_7^+ (m/z 791.21), b_8^+ (m/z 938.34), y_8^+ (m/z 998.54) and y_8^{++} (m/z 499.92), indicating that the loss of 36 Da from the original sequence must have occurred on the subsequence YGLLYC. A new ion with m/z 768.61 is generated through the loss of 230 Da from y_8^+ (Fig. 6), confirmed by MS³ experiments on the y_8^{++} fragment (Fig. 7).

The loss of 230 Da from y_8^+ and y_8^{++} would be consistent with the formation of a vinyl ether between Tyr¹⁶⁴ and a photoproduct of Cys¹⁶⁵ (tentatively assigned to structure **cY**, shown below), and gas phase cleavage of an internal fragment from y_8^+ . The formation of **cY** is rationalized by the conversion of Cys¹⁶⁵ into thioaldehyde (23,37) (see product **7**), followed by thiohemiacetal formation between Tyr¹⁶⁴ and the thioaldehyde, and photo-induced elimination of H₂S (23). This mechanism will be discussed in more detail in the Discussion section).



MS³ experiments on y_8^{++} do not only confirm a neutral loss of 230 Da, but also the formation of the corresponding protonated species, with m/z 231.15 (Fig. 7). In the following, the individual signals in the MS³ spectrum of y_8^{++} will be rationalized with the product ions given in parenthesis: y_8^{++} can cleave Tyr (m/z 835.64) or Phe-Arg (m/z 677.41), where the latter can be followed by cleavage of Tyr-Gly (m/z

457.36), Tyr-Gly-Leu (m/z 344.19) or Tyr-Gly-Leu-Leu (m/z 231.15). The side chain of Arg can cleave (63) the peptide bond C-terminal of Gly, followed by the cleavage of Leu-Leu-**X** (m/z 542.43) and, possibly, Tyr (m/z 379.39). Alternatively, the side chain of Arg can induce cleavage (63) C-terminal of Leu¹⁶³, followed by the loss of **X** (m/z 768.51), or C-terminal of Leu¹⁶², followed by the loss of Leu-**X** (m/z 677.41). Most of these fragments are also present in the MS2 spectrum derived from the ion with m/z 556.78 (Fig. 6). In addition, the MS² spectrum reveals the loss of 287 Da (m/z

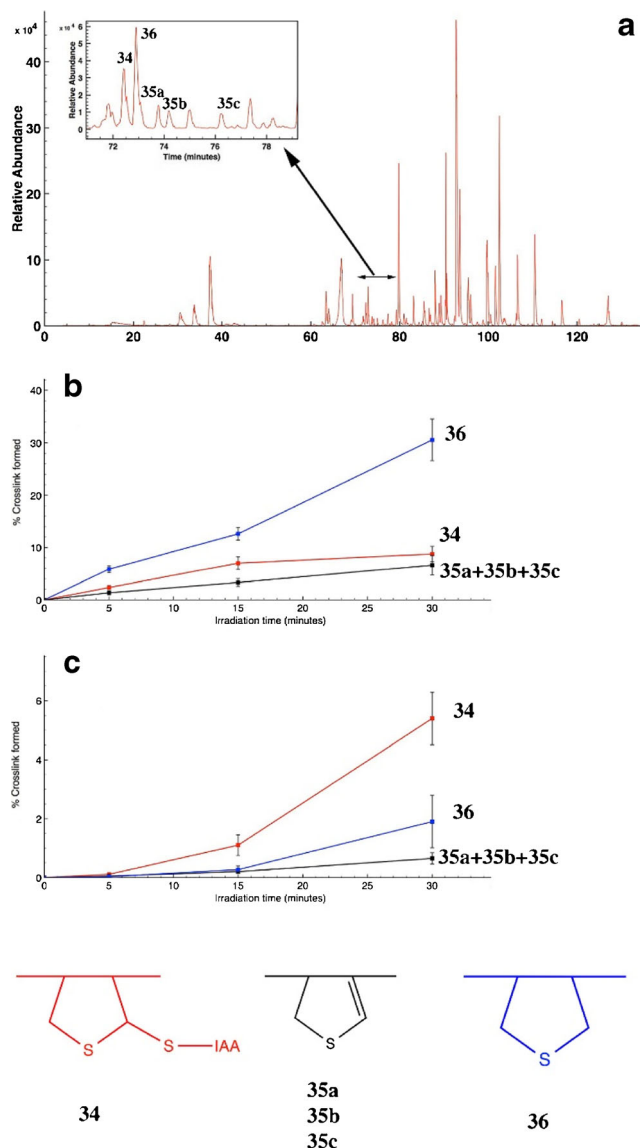


Fig. 10 HPLC-MS analyses on a 75 cm C18 column of the peptide digests of hGH, obtained after photoirradiation of hGH at $\lambda = 254$ nm and $\lambda_{\max} > 295$ nm. **(a)** Resolution of dithiohemiacetal **34** and thioether **36** from three isomers of vinyl thioethers, **35a**, **35b**, and **35c**, obtained after photo-irradiation at $\lambda = 254$ nm. **(b)** Analyses of products **34**, **35a**, **b**, **c**, and **36**, obtained after various times of photo-irradiation of hGH at $\lambda = 254$ nm. **(c)** Analyses of products **34**, **35a**, **b**, **c**, and **36**, obtained after various times of photo-irradiation of hGH at $\lambda > 295$ nm.

825.55) and the presence of an ion with m/z 288.14. This ion would be consistent with an isobaric structure of **X**, generated through a vinyl ether crosslink between Tyr¹⁶⁰ and an oxidation product of Cys¹⁶⁵ (product **46**), connected to Gly¹⁶¹, i.e. Z-G. However, as the formation of Z-G would require multiple gas phase fragmentation processes, and constitutes the only indication for the formation of such isobaric cross-link, additional experimental evidence for such structure would be necessary. MS³ experiments on the ion with m/z 288.14 (Fig. S62), and of the ion with m/z 260 (Fig. S62) were inconclusive.

Additional evidence for the formation of product **45** was obtained in the tryptic fragment T16 + T17, containing one missed cleavage (Fig. S37).

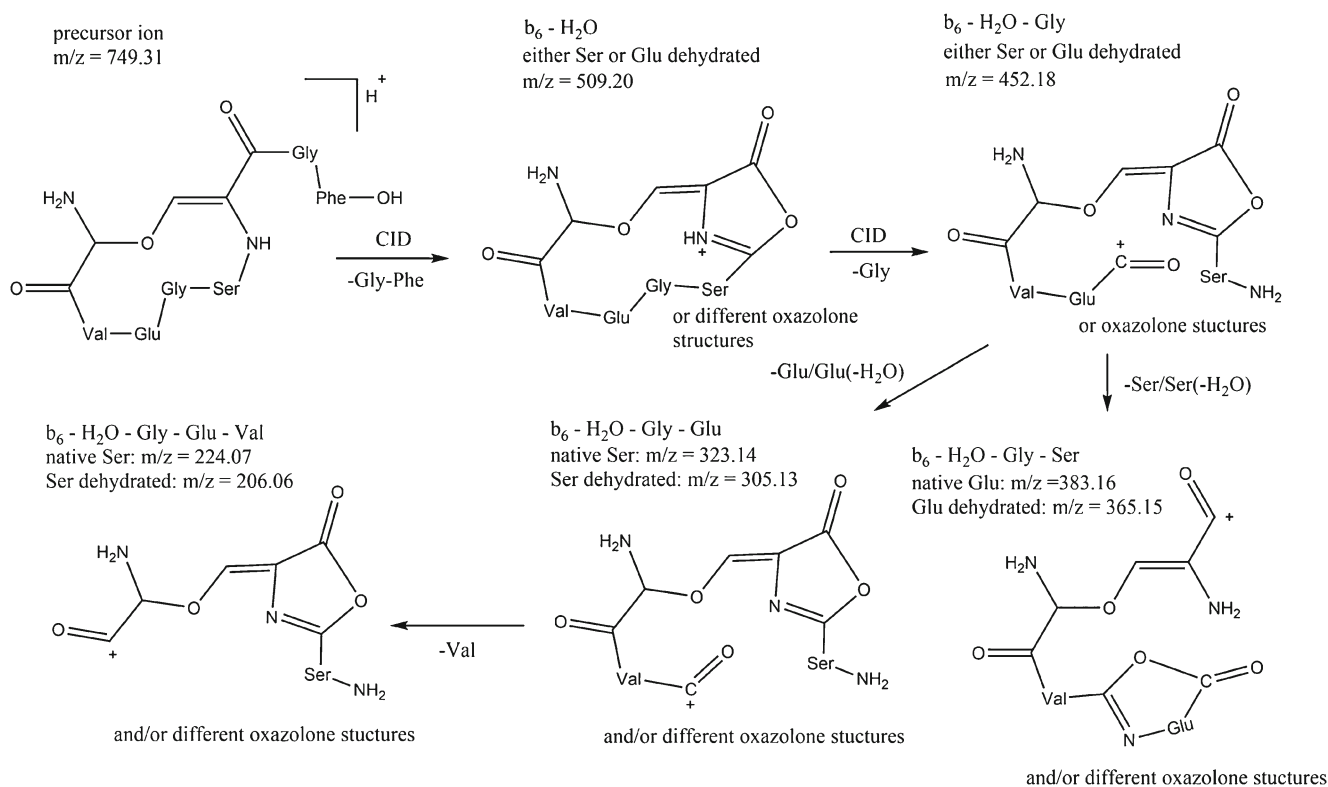
Product **47** represents a putative vinyl thioether cross-link between a thioaldehyde (or its tautomer, 2-amino-3-mercaptoacrylic acid) generated from Cys¹⁶⁵ and dehydrophenylalanine generated from Phe¹⁶⁶. This cross-link would essentially derive from product **15**, which was discussed above. The absence of b2 and y7 ions in the MS/MS spectrum (Fig. S40) of products **15** and **47** would be consistent with such a cross-link.

Product **48** represents a putative cross-link on T6 between a thioaldehyde (or its tautomer, 2-amino-3-mercaptoacrylic acid) generated from Cys⁵³ and dehydrophenylalanine generated from Phe⁵⁴. This cross-link would derive from product **2**, discussed above. The absence of b₁₂ and y₁₁ fragments in the

MS/MS spectrum of products **2** and **48** would be consistent with such a cross-link.

We detected two putative Cys-Trp crosslinks between T9 and T16. One of these cross-links (product **49**) displays the mass of the two tryptic fragments T9 and T16 minus 2 Da. Based on the MS/MS data (Fig. S41), this cross-link is tentatively assigned to a thioether cross-link of Cys¹⁶⁵ with the indole of Trp⁸⁶. Notably, thioether cross-links between Cys and an aromatic amino acid residue, i.e. Tyr, have been detected during the photo-irradiation of insulin (**25**). The other cross-link (product **50**) displays the masses of the two tryptic fragments T9 and T16 minus 34 Da. The MS/MS data (Fig. S42) of product **50** are consistent with a cross-link between Cys¹⁶⁵ and Trp⁸⁶, generated after the loss of H₂S (34 Da). A tentative structure of this cross-link would be a Michael addition product of the indole ring to DHA, generated from Cys¹⁶⁵. The Michael addition of indole to α,β -unsaturated ketones has been reported (64), though unsubstituted indoles tend to add via the C-3 position. In the case of Trp, the indole ring would likely add via the indole nitrogen.

We detected a putative Trp-Tyr crosslink (product **51**) between T9 and T14 which displays the mass of the two tryptic fragments minus 2 Da. The MS/MS data (Fig. S36) of this cross-link are consistent with a covalent bond between Tyr¹⁴³ and Trp⁸⁶, analogous to covalent bonds formed between two Tyr residues in dityrosine cross-links. In fact, trace amounts of such a dityrosine cross-link were detected between tryptic



Scheme I Tentative fragmentation of the cyclic precursor ion with $m/z = 749.31$.

peptides T10 and T14 (product **52**). The MS/MS data of product **52** (Fig. S35) are consistent with a covalent bond between Tyr¹⁴³ and Tyr¹¹¹.

Peptide-Bond-Cleavages

Products derived from peptide bond cleavages are summarized in Table III. We detected an N-terminal cleavage fragment of T6, the peptide Y⁴¹SFLQNPTQTS⁵¹ (product **53**), where the C-terminal Ser⁵¹ displays a carboxylic acid, such as would be expected for peptide bond hydrolysis. This product is absent in non-irradiated controls, indicating that it is not generated through enzymatic processes (e.g., it is not generated during proteolytic digestion). In addition, we detected the same N-terminal cleavage fragment of T6, where the C-terminal Ser⁵¹ is present as an amide, i.e. Y⁴¹SFLQNPTQTS⁵¹-amide (product **54**). An analogous cleavage product of T6 was detected C-terminal of Leu⁵², i.e., the peptide Y⁴¹SFLQNPTQTS⁵²-amide (product **55**). Consistent with the formation of these N-terminal cleavage fragments of T6, we also detected a series of C-terminal cleavage products of T6, i.e. a peptide corresponding to C⁵³(-31 Da)FSESIPTPSNR⁶⁴ (product **56**), a peptide corresponding to F⁵⁴(+26 Da)SESIPTPSNR⁶⁴ (product **57**), and a peptide corresponding to C⁵³(-19 Da)FSESIPTPSNR⁶⁴ (product **58**). In these products, italic one letter codes followed by a mass loss in parenthesis signal a modification to the original amino acid residue. These modifications will be rationalized in the Discussion section.

Two cleavage fragments were also detected for tryptic peptide T16, i.e. N¹⁵⁹YGLLY¹⁶⁴ (product **59**) and N¹⁵⁹YGLLY¹⁶⁴-amide (product **60**).

Time-Dependent Analysis of the Dithiohemiacetal, Thioether, and Vinyl Thioethers on a 75 cm Nano-column

A time-dependent analysis of product formation was carried out representatively for the dithiohemiacetal, thioethers and vinyl thioethers. To better separate potential isomeric products, the photo-irradiated samples were injected onto our in-house packed 75 cm C18 column. Photo-irradiation at $\lambda = 254$ nm led to three isomers of product **35**, referred to as **35a**, **35b**, and **35c** (Fig. 10a). The collision-induced dissociation spectra of **35a**, **35b**, and **35c** were similar to that presented in Fig. S41, consistent with a vinyl thioether structure. Quantitatively, thioether **36** was generated in significantly higher yields compared to products **34** and **35a**, **b**, **c**, when hGH was photo-irradiated at $\lambda = 254$ nm, shown in Fig. 10b, where the respective yields are plotted as a function of irradiation time. In contrast, the dithiohemiacetal **34** was generated at higher yields compared to thioethers and vinyl thioethers, when photo-irradiation was carried out at $\lambda > 295$ nm (Fig.

10c). This is consistent with the light-dependent conversion of dithiohemiacetal into thioether at $\lambda = 254$ nm. (23) Our mechanistic analysis with model peptides (23) revealed that the light-dependent conversion of dithiohemiacetal into thioether proceeds via the intermediary generation of vinyl thioether. Consistent with the intermediacy of vinyl thioethers in the analogous processes in hGH, vinyl thioethers represented the photoproducts with the lowest yields in Fig. 10b and c.

DISCUSSION

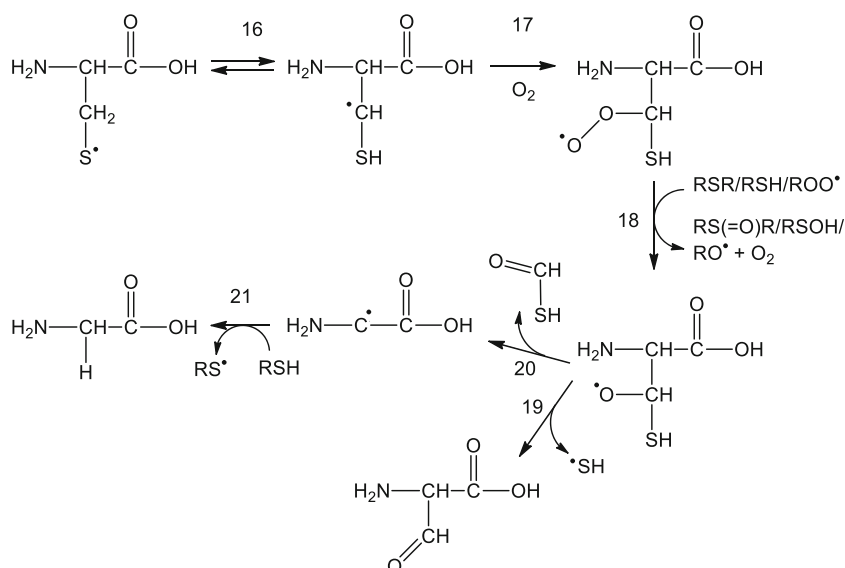
The objective of the present work was to provide a comprehensive characterization of products originating from the photo-degradation of protein disulfides. Hence, this is not a classical pharmaceutical stability study but a forced degradation study applying selected stress conditions (2) for generation of a maximal number of photoproducts.

Mechanistic Considerations

The photo-degradation patterns initiated by UV- irradiation at $\lambda = 254$ nm and $\lambda > 295$ nm are very similar, which suggests common degradation pathways. Indeed, at both wavelengths disulfide bridges of Cys can be cleaved to form CysS[•] radicals (19–22), which are the key intermediates leading to the various products observed (e.g. reactions 7–9). In addition, the aromatic residues of Trp and Tyr can be photo-ionized at both wavelengths, which leads to CysS[•] radicals via the secondary reactions 2, 3, 5 and 6. Once formed, thiolates can be further photo-ionized to CysS[•] radicals (reaction 4) at $\lambda = 230 - 270$ nm (65,66). This likely contributes to the considerably faster photo-degradation at $\lambda = 254$ nm compared to irradiation at $\lambda > 295$ nm. The broad increase in background signals in MS-experiments after irradiation is probably due to the formation of a large number of degradation products of low yields, which could not be identified at present.

Amino Acid Modifications

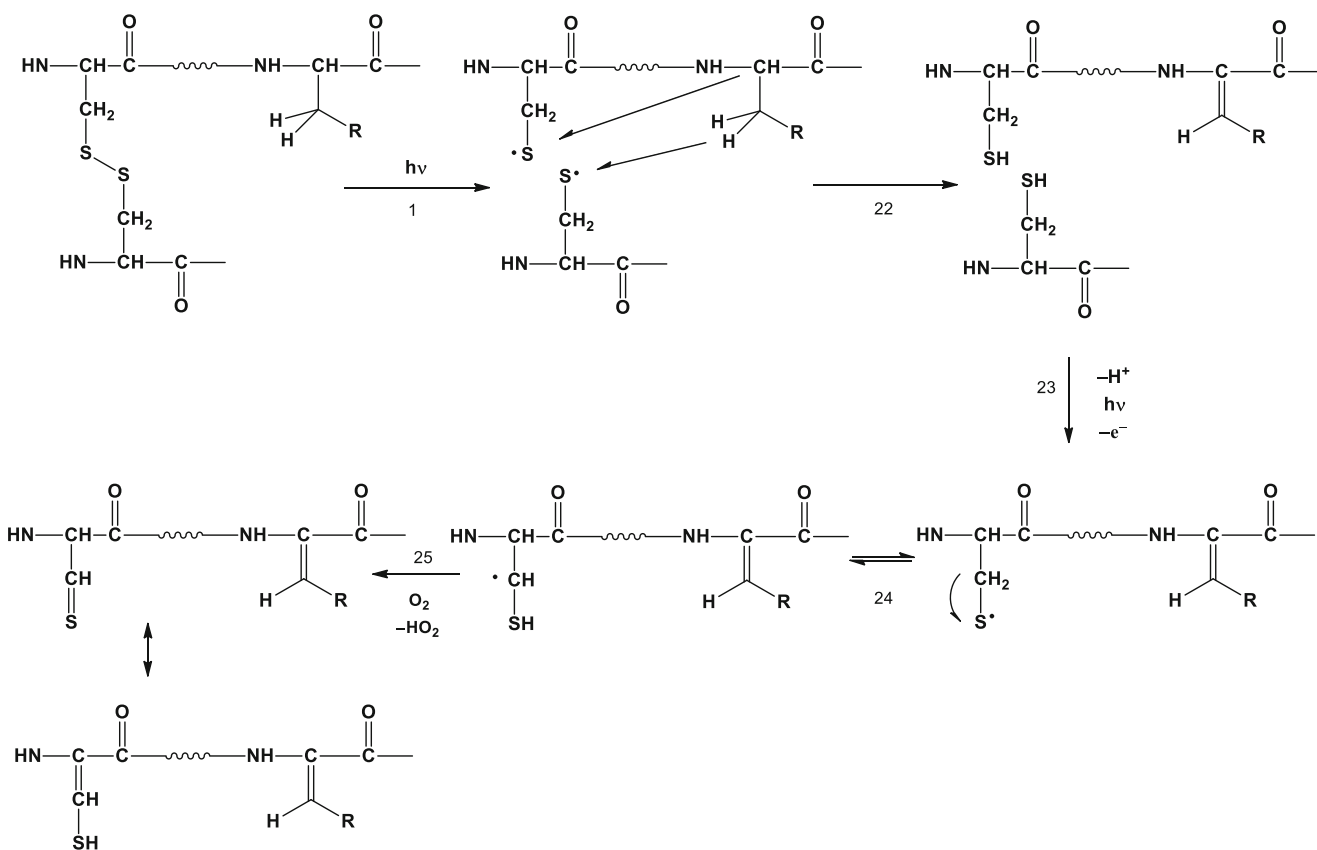
The main degradation products detected were Cys residues alkylated with NEM (products **1**, **6**, **17** and **24**). Cys can be generated by at least three distinct mechanisms: *i*) disproportionation of thiyl radicals to a thiol and thioaldehyde (reaction 7) (23); *ii*) hydrogen transfer (reaction 8) (35–37); and *iii*) equilibrium 3. On the other hand, sulfinic and sulfonic acids (products **8**, **9**, **19**, and **27**) were detected only in minor or trace amounts. They are formed via the reaction of thiyl radicals with oxygen (55,56) or the oxidation of thiols by a variety of oxidizing species such as dioxygen and peroxides (67,68). Furthermore, we detected traces of S-sulfocysteine (product **5**), a product also reported for the photo-irradiation of cysteine (69).

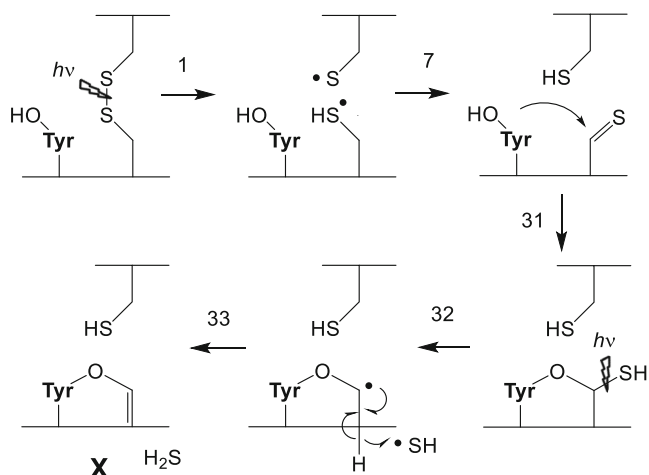
Scheme 2 Tentative mechanism for the conversion of Cys to Gly.

Dha (products **10**, **20**, and **25**) is formed either via the elimination of a sulhydryl radical (HS^\bullet) from a Cys C^α -radical (**23,33**) or via a non-radical dehydrosulfuration reaction during protein digestion (**70**). Since we detected Dha on T16 and T21 in non-irradiated controls both mechanisms likely contribute to the formation of Dha in our experiments. Ala is the reduction product of Dha (**35**), which was detected in products

11 and **18**. The reduction of Dha to Ala likely involves hydrated electrons (**35**) generated during light exposure from thiolate and HS^- (**35**) (formed during dehydrosulfuration of Cys; see above). Such mechanism has been confirmed for the reduction of Dha in small model peptides (**35**).

Thioaldehydes (products **7**, and **28**) generated by reaction **7** were detected as minor product from all Cys-containing

**Scheme 3** Tentative mechanism for the dehydrogenation of two adjacent amino acids.



Scheme 5 Formation of a vinyl ether cross-link between Tyr and a thioaldehyde.

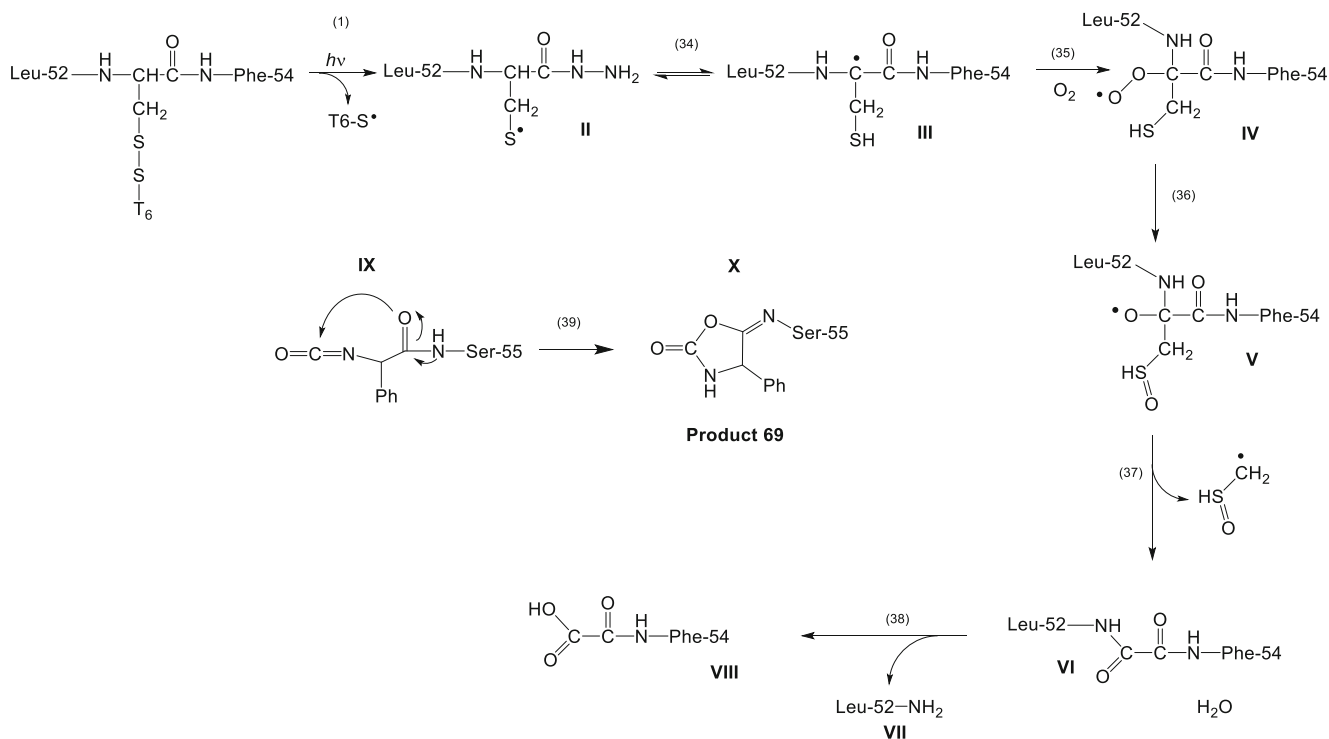
surprising since a major disulfide photo-degradation product is free Cys. We also observed some disulfide scrambling (product **44**) in the non-irradiated control samples, which likely took place during proteolytic digestion. To a much smaller extent, vinyl and divinyl disulfide products were observed (products **37**, **40**, and **41**), that can be generated by reaction of the thioaldehyde tautomer, 2-amino-3-mercaptoacrylic acid, with original disulfides and vinyl disulfide products, respectively.

A novel vinyl ether crosslink was detected on T21 (SVEGSCGF), formed between Ser¹⁸⁴ and a reaction product of Cys¹⁸⁹ (product **38**). The proposed mechanism is shown in

Scheme 4 (part a), and resembles closely our mechanism published for the formation of a vinyl thioether crosslink (**23**): the homolytic cleavage of the disulfide bond (reaction 1) yields a pair of thiyl radicals, followed by disproportionation (reaction 7), and cyclization to yield a thiohemiacetal (reaction 25). The continuous light exposure of the thiohemiacetal leads to elimination of HS• (reaction 26), which abstracts an H-atom to generate H₂S and the vinyl thioether (reaction 27) (**23**). Importantly, additional mechanistic support for this pathway has been derived from studies with Ser and Cys disulfide-containing model peptides, where the intermediary thiohemiacetal was trapped by reaction with NEM (unpublished results). In addition to the mechanism proposed in Scheme 4 (part a), an alternative mechanism can lead to vinyl ether formation through reactions 28–30 (Scheme 4; part b): any radical able to abstract an H-atom from the sulfhydryl group of the thiohemiacetal can generate a thiyl radical (reaction 28), amenable to 1,3-H-transfer (reaction 29) (**33**), followed by the elimination of HS• (reaction 30) (**33**).

The vinyl ethers formed between Tyr¹⁶⁴ and a photoproduct of Cys¹⁶⁵ (product **45**), or Tyr¹⁶⁰ and a photoproduct of Cys¹⁶⁵ (product **46**), are likely generated via an analogous reaction, schematically displayed in Scheme 5 (reactions 31–33). Here, the nucleophilic addition of a phenolic hydroxyl group to a thioaldehyde generates a hemithioacetal, followed by photo-induced release of H₂S.

The disulfide bond between Cys¹⁸² and Cys¹⁸⁹ undergoes photo-induced rearrangement into a dithiohemiacetal crosslink (product **34**), generally formed by nucleophilic attack



Scheme 6 Tentative mechanism leading to peptide cleavage in T6.

of a Cys thiolate on a Cys thioaldehyde (analogous to the reactions presented for Ser in Scheme 4, part a) (23). Under continuous exposure to light, dithiohemiacetals convert into vinyl thioethers (23), which are detected for hGH in products **35** and **39**. The reduction of vinyl thioethers via photolytically generated (e.g., from HS⁻) hydrated electrons leads to thioethers (23). For hGH, such thioether product is detected on T20-T21 (product **36**).

Mechanistically, product **49**, a crosslink between Trp-86 and Cys-165 is likely formed via radical combination of a Trp[•] radical and a Cys[•] radical, as proposed for a Trp-Cys crosslink that was observed during photo-degradation of α -lactalbumin (16). However, also product **50** represents a cross-link between Trp⁸⁶ and a product of Cys¹⁶⁵, which is reduced in mass by 34 Da. This cross-link is likely the product of a Michael-addition (64) via the indole nitrogen of Trp⁸⁶ to DHA (product **10**) formed from Cys¹⁶⁵.

Radical-radical combination reactions between aromatic radicals of Trp and Tyr are most likely responsible for covalent cross-links formed between Trp⁸⁶ and Tyr¹⁴³ (product **51**) and between Tyr¹¹¹ and Tyr¹⁴³ (product **52**).

Cleavage Products

Fragmentation was detected for sequences originally located in tryptic peptides T6 and T16, but not in T20 and T21 (probably due to the small peptide size). Backbone fragmentation via the diamide and α -amidation pathways is well-established in free radical chemistry, and involves the intermediary generation of alkoxy radicals at the C _{α} atom of the respective amino acid residues (41,77). The formation of alkoxy radicals is initiated by H-atom abstraction from C _{α} -H bonds by thiyl radicals, generating [•]C _{α} radicals (78,79). Scheme 6, reaction 34, representatively shows an *intra*-molecular 1,3-H-transfer at the Cys residue, yielding radical **III** (33), but H-atom abstraction from neighboring amino acid residues has been observed as well (35,37,79). The C _{α} radical adds oxygen, yielding peroxy radical **IV** (Scheme 6, reaction 35), which subsequently converts into alkoxy radical **V** through oxygen transfer to the thiol (Scheme 6, reaction 36). Alternative pathways for alkoxy radical formation would include bimolecular reactions of peroxy radicals (41). An α - β -cleavage of the side chain of structure **V** (reaction 37) leads to the oxamide derivative **VI**, which can further hydrolyze (reaction 38) to product **53** (structure **VII**) and product **56** (structure **VIII**). An alternative pathway to product **56** would be the α -amidation pathway (41).

Mechanistically, the formation of products **53** and **54** is related to alkoxy radical formation on the C _{α} atom of Leu⁵². Here, diamide formation and hydrolysis (analogous to reactions 37 and 38) yields product **53** whereas product **54** may be the result of oxamide formation followed by hydrolysis (analogous to reaction 38). An alternative pathway to product **54**

would be the α -amidation pathway (41). Analogous mechanistic considerations apply to the formation of products **59** and **60**, respectively.

Significance

The photo-degradation of hGH at $\lambda = 254$ nm and $\lambda > 295$ nm under forced degradation conditions leads to a large number of disulfide degradation products. A total of 60 products have been identified, and structures tentatively assigned based on MS² and MS³ data. We were able to identify single amino acid modifications, covalent cross-links, and backbone cleavage products. Mechanistically, the formation of several of the observed cross-links required multiple reaction steps such as, e.g., the formation of a dehydroamino acid, followed by the addition of a thioaldehyde tautomer, 2-amino-3-mercaptoacrylic acid, and photo-induced elimination of H₂S. A photo-degradation study such as presented in this paper serves to build a data base of degradation products for the detailed analysis of all types of proteins under various experimental conditions. Future studies need to show whether, and to what extent, some of these products form during manufacturing and storage of protein pharmaceuticals.

ACKNOWLEDGEMENTS

We thank Drs. Mary Cromwell and Jamie Moore for her support of this study and financial support from Genentech, and Dr. Nadya Galeva for the assistance with the mass spectrometric analysis.

REFERENCES

1. Kerwin BA, Remmele RL. Protect from light: photodegradation and protein biologics. *J Pharm Sci.* 2007;96(6):1468–79.
2. Hawe A, Wiggernhorn M, van de Weert M, Garbe JH, Mahler HC, Jiskoot W. Forced degradation of therapeutic proteins. *J Pharm Sci.* 2012;101(3):895–913.
3. Qi P, Volkin DB, Zhao H, Nedved ML, Hughes R, Bass R, *et al.* Characterization of the photodegradation of a human IgG1 monoclonal antibody formulated as a high-concentration liquid dosage form. *J Pharm Sci.* 2009;98(9):3117–30.
4. Sreedhara A, Yin J, Joyce M, Lau K, Weckler AT, Deperalta G, *et al.* Effect of ambient light on IgG1 monoclonal antibodies during drug product processing and development. *Eur J Pharm Biopharm.* 2016;100:38–46.
5. Wei Z, Feng J, Lin H-Y, Mullapudi S, Bishop E, Tous GI, *et al.* Identification of a single tryptophan residue as critical for binding activity in a humanized monoclonal antibody against respiratory syncytial virus. *Anal Chem.* 2007;79(7):2797–805.
6. Lorenz CM, Wolk BM, Quan CP, Alcalá EW, Eng M, McDonald DJ, *et al.* The effect of low intensity ultraviolet-C light on monoclonal antibodies. *Biotechnol Prog.* 2009;25(2):476–82.
7. Liu H, Gaza-Bulsecu G, Zhou L. Mass spectrometry analysis of photo-induced methionine oxidation of a recombinant human monoclonal antibody. *J Am Soc Mass Spectrom.* 2009;20(3):525–8.

8. Haywood J, Mozziconacci O, Allegre KM, Kerwin BA, Schöneich C. Light-induced conversion of Trp to Gly and Gly hydroperoxide in IgG1. *Mol Pharm.* 2013;10(3):1146–50.
9. Bane J, Mozziconacci O, Yi L, Wang YJ, Sreedhara A, Schöneich C. Photo-oxidation of IgG1 and model peptides: detection and analysis of triply oxidized his and trp side chain cleavage products. *Pharm Res.* 2017;34(1):229–42.
10. Donovan JW, Laskowski M, Scheraga HA. Effects of charged groups on chromophores of lysozyme and of amino acids. *J Am Chem Soc.* 1961;83(12):2686.
11. Zhu X, Wentworth P Jr, Wentworth AD, Eschenmoser A, Lerner RA, Wilson IA. Probing the antibody-catalyzed water-oxidation pathway at atomic resolution. *Proc Natl Acad Sci U S A.* 2004;101(8):2247–52.
12. Miller BL, Hageman MJ, Thamann TJ, Barrón LB, Schöneich C. Solid-state photodegradation of bovine somatotropin (bovine growth hormone): Evidence for tryptophan-mediated photooxidation of disulfide bonds. *J Pharm Sci.* 2003;92(8):1698–709.
13. Neves-Petersen MT, Gryczynski Z, Lakowicz J, Fojan P, Pedersen S, Petersen E, *et al.* High probability of disrupting a disulphide bridge mediated by an endogenous excited tryptophan residue. *Protein Sci.* 2002;11(3):588–600.
14. Prompers JJ, Hilbers CW, Pepermans HAM. Tryptophan mediated photoreduction of disulfide bond causes unusual fluorescence behaviour of *Fusarium solani* pisi cutinase. *FEBS Lett.* 1999;456(3):409–16.
15. Vanhooren A, De Vriendt K, Devreese B, Chedad A, Sterling A, Van Dael H, *et al.* Selectivity of tryptophan residues in mediating photolysis of disulfide bridges in goat α -Lactalbumin \dagger . *Biochemistry.* 2006;45(7):2085–93.
16. Vanhooren A, Devreese B, Vanhee K, Van Beeumen J, Hanssens I. Photoexcitation of tryptophan groups induces reduction of two disulfide bonds in goat α -lactalbumin. *Biochemistry.* 2002;41(36):11035–43.
17. Li S, Schöneich C, Borchardt RT. Chemical instability of protein pharmaceuticals: mechanisms of oxidation and strategies for stabilization. *Biotechnol Bioeng.* 1995;48(5):490–500.
18. Grossweiner LI, Kaluskar AG, Baugher JF. Flash photolysis of enzymes. *Int J Radiat Biol.* 1976;29(1):1–16.
19. Creed D. The photophysics and photochemistry of the near-UV absorbing amino acids-III. Cystine and its simple derivatives. *Photochem Photobiol.* 1984;39(4):577–83.
20. Smissman EE, Sorenson JRJ. The electron spin resonance spectra of disulfides irradiated with ultraviolet light. *J Org Chem.* 1965;30(12):4008–10.
21. Joshi A, Yang GC. Spin trapping of radicals generated in the UV photolysis of alkyl disulfides. *J Org Chem.* 1981;46(18):3736–8.
22. Hawari JA, Griller D, Lossing FP. Thermochemistry of perthiyl radicals. *J Am Chem Soc.* 1986;108(12):3273–5.
23. Mozziconacci O, Kerwin BA, Schöneich C. Photolysis of an intrachain peptide disulfide bond: primary and secondary processes, formation of H₂S, and hydrogen transfer reactions. *J Phys Chem B.* 2010;114(10):3668–88.
24. Mozziconacci O, Williams TD, Kerwin BA, Schöneich C. Reversible intramolecular hydrogen transfer between protein cysteine thiyl radicals and alpha C-H bonds in insulin: control of selectivity by secondary structure. *J Phys Chem B.* 2008;112(49):15921–32.
25. Mozziconacci O, Haywood J, Gorman EM, Munson E, Schöneich C. Photolysis of recombinant human insulin in the solid state: formation of a dithiohemiacetal product at the C-terminal disulfide bond. *Pharm Res.* 2012;29(1):121–33.
26. Mozziconacci O, Schöneich C. Photodegradation of oxytocin and thermal stability of photoproducts. *J Pharm Sci.* 2012;101(9):3331–46.
27. Hoffman MZ, Hayon E. One-electron reduction of the disulfide linkage in aqueous solution. Formation, protonation, and decay kinetics of the RSSR \cdot radical. *J Am Chem Soc.* 1972;94(23):7950–7.
28. Purdie JW, Gillis HA, Klassen NV. The pulse radiolysis of penicillamine and penicillamine disulfide in aqueous solution. *Can J Chem.* 1973;51(18):3132–42.
29. Koppenol WH. Oxyradical reactions: from bond-dissociation energies to reduction potentials. *FEBS Lett.* 1990;264(2):165–7.
30. Nauser T, Koppenol WH, Gebicki JM. The kinetics of oxidation of GSH by protein radicals. *Biochem J.* 2005;392(3):693–701.
31. Prütz WA, Butler J, Land EJ, Swallow AJ. The role of sulphur peptide functions in free radical transfer: a pulse radiolysis study. *Int J Radiat Biol.* 1989;55(4):539–56.
32. Macrae RM, Carmichael I. Density functional studies of hydrogen atom addition to the C=S bond. *J Phys Chem A.* 2001;105(14):3641–51.
33. Nauser T, Koppenol WH, Schöneich C. Reversible hydrogen transfer reactions in thiyl radicals from cysteine and related molecules: absolute kinetics and equilibrium constants determined by pulse radiolysis. *J Phys Chem B.* 2012;116(18):5329–41.
34. Mozziconacci O, Williams TD, Kerwin BA, Schöneich C. Reversible intramolecular hydrogen transfer between protein cysteine thiyl radicals and α C–H bonds in insulin: control of selectivity by secondary structure. *J Phys Chem B.* 2008;112(49):15921–32.
35. Mozziconacci O, Kerwin BA, Schöneich C. Reversible hydrogen transfer reactions of cysteine thiyl radicals in peptides: the conversion of cysteine into dehydroalanine and alanine, and of alanine into dehydroalanine. *J Phys Chem B.* 2011;115(42):12287–305.
36. Nauser T, Casi G, Koppenol WH, Schöneich C. Reversible intramolecular hydrogen transfer between cysteine thiyl radicals and glycine and alanine in model peptides: absolute rate constants derived from pulse radiolysis and laser flash photolysis. *J Phys Chem B.* 2008;112(47):15034–44.
37. Mozziconacci O, Kerwin BA, Schöneich C. Reversible hydrogen transfer between cysteine thiyl radical and glycine and alanine in model peptides: covalent H/D exchange, radical–radical reactions, and l- to d-Ala conversion. *J Phys Chem B.* 2010;114(19):6751–62.
38. Headlam HA, Mortimer A, Easton CJ, Davies MJ. β -scission of C-3 (β -carbon) alkoxy radicals on peptides and proteins: a novel pathway which results in the formation of α -carbon radicals and the loss of amino acid side chains. *Chem Res Toxicol.* 2000;13(11):1087–95.
39. Headlam HA, Davies MJ. Beta-scission of side-chain alkoxy radicals on peptides and proteins results in the loss of side-chains as aldehydes and ketones. *Free Radic Biol Med.* 2002;32(11):1171–84.
40. Requena JR, Levine RL, Stadtman ER. Recent advances in the analysis of oxidized proteins. *Amino Acids.* 2003;25(3-4):221–6.
41. Garrison WM. Reaction mechanisms in the radiolysis of peptides, polypeptides, and proteins. *Chem Rev.* 1987;87(2):381–98.
42. Cheng E, Jinzenji D, Lorthiois A, Carvalho R, Tanaka-Azevedo A, Raw I, *et al.* Purification of coagulation factor VIII using chromatographic methods. Direct chromatography of plasma in anion exchange resins. *Biotechnol Lett.* 2010;32(9):1207–14.
43. Ansorena E, Garbayo E, Lanciego JL, Aymerich MS, Blanco-Prieto M. Production of highly pure human glycosylated GDNF in a mammalian cell line. *Int J Pharm.* 2010;385(1–2):6–11.
44. Steinmann D, Ji JA, Wang YJ, Schöneich C. Photodegradation of human growth hormone: a novel backbone cleavage between Glu-88 and Pro-89. *Mol Pharm.* 2013;10(7):2693–706.
45. Forum UP. In: *The United States Pharmacopeia (1990)*. Easton: Mack Printing Co; 1989. p. 1246.
46. Company SNEU. Model RPR-100. 2012. Available from: <http://www.rayonet.org/Page%20REACTORS/RPR-100pdf.pdf>.
47. Administration FaD. Photostability testing of new drug substances and products. In: *Services DoHaH, editor.*; 1997. p. 27115–27122.

48. Ikehata K, Duzhak TG, Galeva NA, Ji T, Koen YM, Hanzlik RP. Protein targets of reactive metabolites of thiobenzamide in rat liver in vivo. *Chem Res Toxicol*. 2008;21(7):1432–42.
49. Xu H, Freitas MA. Monte Carlo simulation-based algorithms for analysis of shotgun proteomic data. *J Proteome Res*. 2008;7(7):2605–15.
50. Grinias KM, Godinho JM, Franklin EG, Stobaugh JT, Jorgenson JW. Development of a 45kpsi ultrahigh pressure liquid chromatography instrument for gradient separations of peptides using long microcapillary columns and sub-2 μ m particles. *J Chromatogr A*. 2016;1469:60–7.
51. Wright SK, Viola RE. Evaluation of methods for the quantitation of cysteines in proteins. *Anal Biochem*. 1998;265(1):8–14.
52. Steinmann D, Ji JA, Wang YJ, Schöneich C. Oxidation of human growth hormone by oxygen-centered radicals: formation of Leu-101 hydroperoxide and Tyr-103 oxidation products. *Mol Pharm*. 2012;9(4):803–14.
53. Baldwin AD, Küick KL. Tunable degradation of maleimide–thiol adducts in reducing environments. *Bioconjug Chem*. 2011;22(10):1946–53.
54. Everett SA, Schöneich C, Stewart JH, Asmus KD. Perthiyl radicals, trisulfide radical ions, and sulfate formation - a combined photolysis and radiolysis study on redox processes with organic disulfides and trisulfides. *J Phys Chem*. 1992;96(1):306–14.
55. Sevilla MD, Becker D, Swarts S, Herrington J. Sulfinyl radical formation from the reaction of cysteine and glutathione thiyl radicals with molecular oxygen. *Biochem Biophys Res Commun*. 1987;144(2):1037–42.
56. Sevilla MD, Becker D, Yan M. The formation and structure of the sulfoxyl radicals RSO(\cdot), RSOO(\cdot), RSO2(\cdot), and RSO2OO(\cdot) from the reaction of cysteine, glutathione and penicillamine thiyl radicals with molecular oxygen. *Int J Radiat Biol*. 1990;57(1):65–81.
57. Forbes WF, Rivett DE, Savige WE. Photolysis and photo-oxidation of amino acids and peptides. 3. Effect of ionizing radiation on cystine and related amino acids. *Photochem Photobiol*. 1962;1(2):97–103.
58. Dose K, Rajewsky B. Photochemistry of sulphur containing amino acids and peptides. *Photochem Photobiol*. 1962;1(2):181–9.
59. Asquith RS, Shah AV. Photochemical degradation of cystine in aqueous solutions in presence of nitrogen. *Biochim Biophys Acta*. 1971;244(3):547.
60. Russell GA. Deuterium-isotope effects in the autoxidation of aralkyl hydrocarbons - mechanism of the interaction of peroxy radicals. *J Am Chem Soc*. 1957;79(14):3871–7.
61. Mozziconacci O, Kerwin BA, Schöneich C. Exposure of a monoclonal antibody, IgG1, to UV-light leads to protein dithiohemiacetal and thioether cross-links: a role for thiyl radicals? *Chem Res Toxicol*. 2010;23(8):1310–2.
62. Datola A, Richert S, Bierau H, Agugiario D, Izzo A, Rossi M, et al. Characterisation of a novel growth hormone variant comprising a thioether link between Cys182 and Cys189. *ChemMedChem*. 2007;2(8):1181–9.
63. Paizs B, Suhai S. Fragmentation pathways of protonated peptides. *Mass Spectrom Rev*. 2005;24(4):508–48.
64. Wang SY, Ji SJ, Loh TP. The Michael addition of indole to alpha, beta-unsaturated ketones catalyzed by iodine at room temperature. *Synlett*. 2003;15:2377–9.
65. Rosengren KJ. The photolysis of alkanethiols in a rigid glass at 77 degrees K with the possible formation of thiyl radicals. *Acta Chem Scand*. 1962;16:1418–20.
66. Caspari G, Granzow A. The flash photolysis of mercaptans in aqueous solution. *J Phys Chem*. 1970;74(4):836–9.
67. Bagiyan GA, Koroleva IK, Soroka NV, Ufimtsev AV. Oxidation of thiol compounds by molecular oxygen in aqueous solutions. *Russ Chem Bull*. 2003;52(5):1135–41.
68. Turell L, Boti H, Carballal S, Ferrer-Sueta G, Souza JM, Duran R, et al. Reactivity of sulfenic acid in human serum albumin. *Biochemistry*. 2007;47(1):358–67.
69. Forbes WF, Savige WE. Photolysis and photo-oxidation of amino acids and peptides-I. Irradiation of aqueous solutions of cystine with sunlight and other ultraviolet light sources. *Photochem Photobiol*. 1962;1(1):1–13.
70. Wang Z, Rejtar T, Zhou ZS, Karger BL. Desulfurization of cysteine-containing peptides resulting from sample preparation for protein characterization by mass spectrometry. *Rapid Commun. Mass Spectrom*. 2010;24(3):267–75.
71. Bothe E, Behrens G, Schultefrohlinde D. Mechanism of 1st order decay of 2-hydroxy-propyl-2-peroxyl radicals and of O₂-formation in aqueous-solution. *Z Naturforsch B*. 1977;32(8):886–9.
72. Bothe E, Schuchmann MN, Schultefrohlinde D, Vonsontag C. Ho₂ elimination from alpha-hydroxyalkylperoxyl radicals in aqueous-solution. *Photochem Photobiol*. 1978;28(4-5):639–44.
73. Bothe E, Schultefrohlinde D, Sonntag CV. Radiation-chemistry of carbohydrates. 16. Kinetics of Ho₂ elimination from peroxy radicals derived from glucose and polyhydric alcohols. *J Chem Soc, Perkin Trans 2*. 1978;5(5):416–420.
74. Von Sonntag C, Dowideit P, Fang X, Mertens R, Pan X, Schuchmann MN, et al. The fate of peroxy radicals in aqueous solution. *Water Sci Technol*. 1997;35(4):9–15.
75. Schöneich C, Aced A, Asmus KD. Halogenated peroxy radicals as 2-electron-transfer agents - oxidation of organic sulfides to sulfoxides. *J Am Chem Soc*. 1991;113(1):375–6.
76. Mozziconacci O, Schöneich C. Effect of conformation on the photodegradation of Trp- and cystine-containing cyclic peptides: octreotide and somatostatin. *Mol Pharm*. 2014;11(10):3537–46.
77. Davies MJ. The oxidative environment and protein damage. *Biochim Biophys Acta*. 2005;1703(2):93–109.
78. Nauser T, Schöneich C. Thiyl radicals abstract hydrogen atoms from the (alpha)C-H bonds in model peptides: absolute rate constants and effect of amino acid structure. *J Am Chem Soc*. 2003;125(8):2042–3.
79. Mozziconacci O, Sharov V, Williams TD, Kerwin BA, Schöneich C. Peptide cysteine thiyl radicals abstract hydrogen atoms from surrounding amino acids: the photolysis of a cystine containing model peptide. *J Phys Chem B*. 2008;112(30):9250–7.
80. El Aribi H, Orlova G, Hopkinson AC, Siu KWM. Gas-phase fragmentation reactions of protonated aromatic amino acids: concomitant and consecutive neutral eliminations and radical cation formations. *J Phys Chem A*. 2004;108(17):3844–53.